# Calculated effective Hamiltonian for $La_2CuO_4$ and solution in the impurity Anderson approximation

A. K. McMahan
*Lawrence Livermore National Laboratory, University of California, Livermore, California 94550*

Richard M. Martin
*Department of Physics, University of Illinois, Urbana, Illinois 61801*

S. Satpathy
*Department of Physics and Astronomy, University of Missouri, Columbia, Columbia, Missouri 65211*

(Received 10 May 1988)

We report local-density-functional calculations of hybridization matrix elements and effective electron-electron interactions in $La_2CuO_4$ defining a general effective Hamiltonian that we propose as an appropriate starting point for many-body calculations in this material. The parameter values lend support to an Anderson lattice model. We find the impurity approximation to this model yields a magnetic ground state of $x^2-y^2$ symmetry, a 1–2-eV insulating gap bounded by ionization and affinity levels of the same symmetry, and a calculated $d$ spectral weight in qualitative agreement with photoemission experiments. We discuss anticipated modification of these results by lattice effects.

## I. INTRODUCTION

The nature of the electronic states in strongly correlated systems, such as transition-metal oxides and rare-earth compounds, pose key issues in condensed-matter physics.[1–3] New stimulus for understanding these issues has been provided by the discovery of superconductivity at high temperature in compounds containing copper-oxygen planes.[4–6] Within this class of materials there is variation from antiferromagnetically ordered insulators[7] to superconductors, in which there is evidence for local magnetic moments with short-range antiferromagnetic correlations.[8] Therefore, we now wish to understand not only the magnetic and metal-insulator transitions that are characteristic of transition-metal oxides, but also the relation of their underlying electronic properties to superconductivity.

Many different proposals have been made for electronic mechanisms that can lead to superconductivity in the copper oxide materials. Anderson[9] has proposed that a "resonating-valence-bond" state occurs in two-dimensional one-band systems due to on-site repulsive interactions. Much work has investigated the pairing and excitations in such models.[10,11] Other papers have proposed that it is essential to include at least two bands with holes existing in oxygen states correlated with spins centered on copper sites.[12–16] Superconducting solutions have been suggested for a multiband Anderson lattice-type model.[17,18] In contrast, mechanisms for superconductivity based upon charge-fluctuation-induced pairing depend upon the magnitudes of Coulomb interactions between different states.[19–23] The complexity of the problem has made it difficult to choose from these and other[24–27] very different models of the electronic structure.

The purpose of the present paper is to carry out quantitative theoretical investigations of the electronic structure and interactions in representative cases for the copper-oxide-based materials.[4–6] We utilize *ab initio* techniques, which have been developed to the point where realistic predictions can now be made for many material properties of solids. The most widely used method is the density-functional theory[28,29] which has been very successful in describing the electronic properties of materials with wide electronic bands.[30] In these systems the electronic correlations are well represented by local charge-density and spin-density functionals, and detailed calculations can be carried out on realistic systems. A number of such calculations have been published for the $La_2CuO_4$ superconductor.[31–36] This work provides us with our basic picture of the electronic states; nevertheless, it is unsatisfying because the density-functional approach is inadequate to treat correlation effects in narrow bands. Well known examples of such effects occur in mixed-valence and heavy-fermion rare-earth materials, where many-body effects cause very large renormalizations of the electronic states and can lead to ground states different from those predicted by the local-density-functional calculations.[2]

Strongly correlated materials have been approached by different methods to better treat the many-body electron system. These include quantum Monte Carlo simulations,[37,38] configuration-interaction techniques,[39] and analytical approaches.[40,41] Among the last are included the $(1/N)$ expansion methods which have been widely used in the heavy-fermion problems.[42] In particular, essentially exact solutions for realistic many-body impurity problems have been made possible by the methods pioneered by Gunnarsson and Schönhammer.[40]

In this paper we report calculations on $La_2CuO_4$, which are representative of cases in which the dominant electronic features are associated with planes formed of Cu and O. We utilize the density-functional method in two ways: One way is to produce the ordinary self-consistent local-density-functional solution for the ground state,

 

which provides an approximate band structure and estimates of hybridization matrix elements between neighboring O(2$p$)-O(2$p$) and Cu(3$d$)-O(2$p$) orbitals. This is similar to previous work,[31-36] although we emphasize the strong O(2$p$)-O(2$p$) overlap which has not generally been appreciated, and we provide the first calculations for $La_2CuO_4$ of the symmetry decomposed hybridization functions between local Cu(3$d$) orbitals and the itinerant O(2$p$) band. The second way is to carry out total-energy calculations with constrained occupations, which leads to effective electron-electron interactions. This method has been shown by ourselves[43] and others[44-46] to be very powerful for rare-earth compounds[43-45] and NiO.[44,46] Similar calculations in addition to the present work are now being applied to the new copper oxide materials.[47,48] The combined results of these two applications of local-density-functional theory lead to quantitative values for terms in the effective interacting-electron Hamiltonian describing the electrons in $La_2CuO_4$. This result which is described in Sec. II is one of the primary results of our work. We believe our results suggest appropriate forms for Hamiltonians that can be used in many-body calculations which can then describe the many-body interacting system.

The parameter values lend support to an Anderson lattice model for $La_2CuO_4$, by which we mean small direct Cu(3$d$)-Cu(3$d$) coupling, large O(2$p$) bandwidth, and small Coulomb interactions on the O sites. The last of the three criteria, it should be noted, may only be marginally satisfied in the present case. As this model is still extremely difficult to solve, we proceed in Sec. III to calculate the ground state and excitation spectra for the many-body system by making the impurity approximation and using the methods of Gunnarsson and Schönhammer.[40,41] This impurity ansatz is expected to give accurate results for some properties, in particular, the high-energy "satellites" in the response function for removing electrons. By comparing with experimental photoemission spectra,[49-53] we show that the data support our calculated interactions. The impurity-model calculations lead to a magnetic ground state of $x^2-y^2$ symmetry, and a 1-2-eV insulating gap bounded by ionization and affinity levels for which the added hole or electron is in each case of this same symmetry. The added hole in the first ionization level forms a singlet state in cooperation with an existing hole of the intrinsic material. For these results, however, we must be careful to recognize differences between the impurity and the actual lattice that exists in the real material, an issue we turn to in Sec. IV, where we also summarize the results of our paper and speculate on the nature of the electronic states in the lattice case and the appropriate effective Hamiltonian for many-body calculations.

## II. CALCULATION OF PARAMETERS FOR AN EFFECTIVE HAMILTONIAN

This section describes local-density-functional calculations which are used to determine parameters entering a general effective Hamiltonian for $La_2CuO_4$. The self-consistent ground-state band structure is analyzed in Sec. II A to provide approximate O(2$p$)-O(2$p$) and O(2$p$)-Cu(3$d$) hybridization matrix elements. Constrained-occupation total-energy calculations used to determine the effective electron-electron interactions are presented in Sec. II B, while the full effective many-body Hamiltonian which results from these combined calculations is summarized in Sec. II C. The impurity Anderson approximation to the full Hamiltonian requires symmetry-decomposed hybridization functions which may be determined from the approximate matrix elements given in Sec. II A, or by more accurate direct calculations as described in Sec. II D.

TABLE I. Basis and sphere sizes for LMTO calculations of bct $La_2CuO_4$. The sphere radii $R$ in bohrs; the basis positions, in units of $a$ or $c$. The lattice constant was taken $a=7.212$ bohrs; $c/a=3.4567$. ES signifies empty sphere.

| Atom | $R$ | Basis positions | |
|---|---|---|---|
| Cu | 2.48 | (0,0,0) | |
| La | 3.59 | (0.0,0.362) | (0,0,−0.362) |
| $O_I$ | 1.98 | (0,0.5,0) | (0.5,0,0) |
| $O_{II}$ | 1.98 | (0,0,0.182) | (0,0,−0.182) |
| ES | 2.00 | (0,0.5,0.25) | (0.5,0,−0.25) |

We have used the linear muffin-tin orbitals[54-56] (LMTO) implementation of local-density-functional theory in our band structure and total energy calculations for $La_2CuO_4$. Calculations for the body-centered-tetragonal (bct) structure of $La_2CuO_4$ were carried out using the sphere radii listed in Table I, including two empty spheres as in the manner of Oguchi.[34] In this table, and throughout this paper, we denote O sites in the $CuO_2$ layers as $O_I$; those outside these layers, as $O_{II}$. For tests in which the Cu-sphere radii are increased by 10% (20%), we reduce each of the La, O, and empty-sphere radii by 1.22% (2.73%) in order to preserve cell volume. All calculations were scalar relativistic, retaining all relativistic effects except spin orbit, and employed the exchange-correlation potential of von Barth and Hedin.[57] Self-consistency was generally achieved using 18 points per irreducible wedge of the bct Brillouin zone, as tests with 75 points per wedge led to negligible differences. The combined correction was not included, except in tests as noted. One panel was used for the Cu(3$d$)-O(2$p$) bands, and a second panel for the lower-lying La(5$p$) and O(2$s$) bands. Angular momentum components $s,p,\ldots,l_{\max}$ were taken within the spheres where $l_{\max}=d$ (Cu), $f$ (La), $p$ (O and empty spheres) for the upper panel, and $l_{\max}=p$ in all cases for the lower panel. Only small changes result from larger limits. Reduction of $l_{\max}$ from $d$ to $p$ for the Cu spheres provides a convenient way to eliminate Cu(3$d$) components from the bands. In the original LMTO formulation[54,55] used here except where indicated, the limits $l_{\max}$ are applied to the structure constants, and thus separately to both the Hamiltonian and overlap matrices. The newer formulation[56] with screened structure constants provides a nearly orthogonal basis in which there is no overlap matrix.

### A. Band structure and approximate hybridization matrix elements

The local-density-calculated electron-band structure for $La_2CuO_4$ has already been discussed in the litera-

ture.[31-36] The most prominent feature is the antibonding band at the top of the combined Cu($3d$) and O($2p$) bands which rises above the Fermi level at the $X$ point, as seen in Fig. 1(a). A tight-binding model with a single $V_{pd\sigma}$ interaction between neighboring Cu and O atoms reproduces this feature as noted by Mattheiss.[31] This simple $V_{pd\sigma}$ abstraction of the electronic structure has been an underlying assumption for numerous theoretical papers on the new superconductivity.

The first point which we wish to emphasize here is that the oxygen-derived bands have a significant width independent of the Cu $d$ states, a fact which is now gaining acceptance.[17,18,26,27] This is already suggested in Fig. 1(a) and by results of Refs. 31-36 from the width of the bands at the $\Gamma$ point, although the choice of different centers for the Cu and two types of O states can also contribute to this width. It is instructive to make this more quantitative by explicitly decoupling the Cu $d$ states. In Fig. 1(b) we show the results of bands calculated in exactly the same potential as for Fig. 1(a), but with the Cu $d$ states simply removed. The 12 remaining valence levels range from $-9.3$ to $-2.6$ eV and are primarily of O($2p$) character mixed with all other states except Cu $d$. The bandwidth of 6.7 eV results almost entirely from hybridization width and is primarily from direct $p$-$p$ interactions between neighboring O atoms. This may be seen from calculations which exclude all states except those of $p$ character in the O spheres, which lead to a bandwidth of 6.3 eV, almost as large as the full width. Widths of this magnitude are expected based upon simple size arguments for the large $O^{2-}$ ion. An even larger width is predicted by Harrison's general expressions[58] for the matrix elements, given the observed O-O separations.

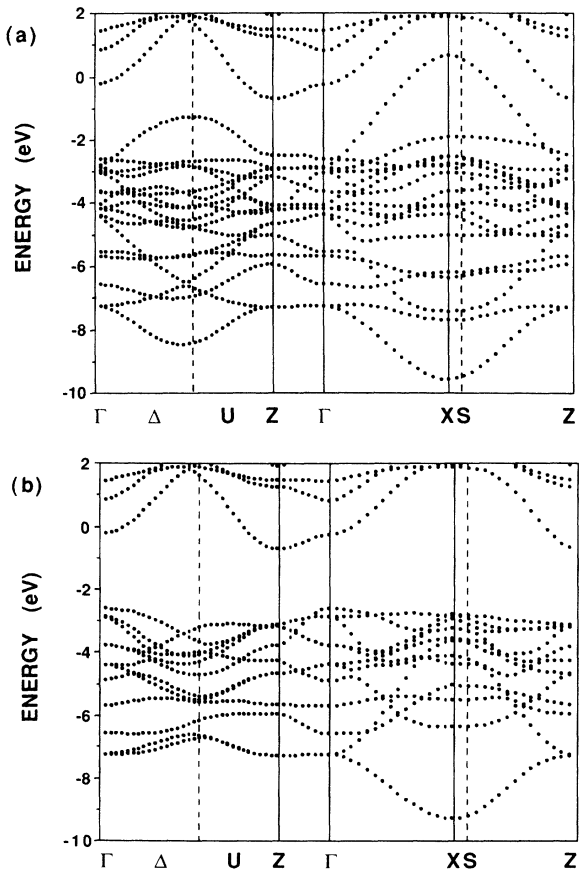


FIG. 1. (a) Local-density band structure for $La_2CuO_4$. (b) O($2p$) and conduction bands above obtained from the same one-electron potential used in (a), but with Cu($3d$) components eliminated.

Some understanding of the O bands in Fig. 1(b) is provided by Fig. 2, which sketches the bands arising from near-neighbor interactions of a two-dimensional square O lattice, as occurs in the $CuO_2$ layers. In the $La_2CuO_4$ structure, the doubly degenerate states at $X$ are split, and may conveniently be classified by their transformation properties about the Cu sites, as shown by the orbital sketches to the right of Fig. 2. These states may be identified in Fig. 1(b) as follows: $d_{x^2-y^2}$ ($-2.9$ eV), $g_{xy(x^2-y^2)}$ ($-3.6$ eV), $d_{xy}$ ($-6.3$ eV), and $s$ or $d_{3z^2-r^2}$ ($-9.3$ eV). A notation in current use[15,27] labels that $p_x$ or $p_y$ orbital at each $O_I$ site which points *at* its near-neighbor Cu sites as $p_\sigma$, the other, $p_\pi$. The four states just listed are then $p_\sigma$ antibonding, $p_\pi$ antibonding, $p_\pi$ bonding, and $p_\sigma$ bonding molecular orbitals, respectively. Of the remaining 8 levels at $X$, two involve $p_z$ orbitals of the $O_I$ (in-plane) atoms, while the rest are predominantly of $O_{II}(2p)$ character. The $-2.9$-eV energy of the $O_I(2p)$ antibonding $d_{x^2-y^2}$ molecular orbital lies close to the top ($-2.6$ eV) of the combined O($2p$) bands in Fig. 1(b), so that $O_I(2p)$ state density is distributed throughout essentially the full width of these bands. States of predominantly $O_{II}(2p)$ character occur largely in the upper third of this range, including, for example, levels at $\Gamma$ above about $-4$ eV.

The width of the two-dimensional O bands in Fig. 2 is $4(V_{pp\sigma}+V_{pp\pi})$ at $\Gamma$, and $4(V_{pp\sigma}-V_{pp\pi})$ at $X$, in terms of the usual Slater-Koster parameters.[59] The separation between the doubly degenerate $O_I(2p)$ levels at $\Gamma$ in Fig. 1(b) is $4(V_{pp\sigma}+V_{pp\pi})=2.9$ eV, giving $V_{pp\sigma}\approx 1.0$ eV and $V_{pp\pi}\approx -0.3$ eV. These values are a compromise between taking the width at $X$ as the distance between the average (over $p_\sigma$ and $p_\pi$) antibonding and bonding levels mentioned above, or using just the more distance $p_\sigma$ levels. Combined with the LMTO band centers (orbital energies at which the logarithmic derivatives $=-l-1$) $C_{Ip}=-5.3$ eV and $C_{IIp}=-3.5$ eV, these parameter values yield the gross features of the full $La_2CuO_4$ O($2p$) bands in a tight-binding calculation including all near-neighbor $O_I$-$O_I$, $O_I$-$O_{II}$, and $O_{II}$-$O_{II}$ pairs, and scaling the $V$'s by $d^{-l-l'-1}=d^{-3}$ to the larger O-O distances.

The intrinsic Cu($3d$) width is a bit more sensitive to the choice of basis, but appears to be $\approx 1$ eV. The five Cu($3d$) bands obtained from LMTO calculations which prohibit $p$ components in the O spheres give a 1.3 eV width, while unhybridized calculations allowing only $d$ components in the Cu spheres give 0.3 eV. The two limits correspond roughly to Cu($3d$) Wannier functions which in the first case have tails extending into neighboring O spheres, and in the second case do not. Similar calculations with the newer orthogonal formulation[56] of the muffin-tin-orbital basis offer more of a compromise between the two limits, and yield closer numbers (1.2 and

0.7 eV, respectively).

Turning now to the Cu($3d$)-O($2p$) hybridization, we note that the Cu($3d$) states (band center $C_d = -4.1$ eV) lie near the top of the O($2p$) bands, close to the antibonding $O_I(2p)$ molecular orbital of $d_{x^2-y^2}$ symmetry at $-2.9$ eV. This explains why the $d_{x^2-y^2}$ Cu-O antibonding hybrid rises well above the combined bands as seen near $X$ in Fig. 1(a). The $d_{x^2-y^2}$ Cu-O bonding counterpart can be seen in the downward reflection of this shape, broken into segments by its mixing with O states, and reaching down to about the *second* lowest band at $X$. The lowest level at $X$ in Fig. 1(a) has 29% Cu-$s$, but only 7% Cu-$d$ character, and thus remains the $s$-like O—O bonding state sketched in Fig. 2. This band near $X$, and the full width of the bands at $\Gamma$, are due predominantly to the strong O-O overlap.

The $X$ point $d_{x^2-y^2}$ Cu—O bonding-antibonding separation is approximately $2\sqrt{6}V_{pd\sigma}$. Taking the highest and second lowest of the 17 Cu($3d$)-O($2p$) bands at $X$ in Fig. 1(a), this suggests $V_{pd\sigma} \approx -1.7$ eV, which is close to our more accurate result $V_{pp\sigma} = -1.85$ eV (also $V_{pp\pi} = 0.75$ eV) obtained later on in Sec. II D. Table II collects together the hybridization matrix elements $V$ and band centers $C$ which provide a gross representation of our combined Cu($3d$) and O($2p$) bands in $La_2CuO_4$.

### B. Total-energy calculations of electron-electron interactions

In this subsection we describe calculations of effective electron-electron interactions following our previous work[43] on related systems. The basic idea is to isolate an orbital so that it is not hybridized with others. Since its occupation $n$ is then a good quantum number, we may calculate the density-functional total energy $E(n)$ as a function of $n$, and thus determine the Coulomb interactions $U$

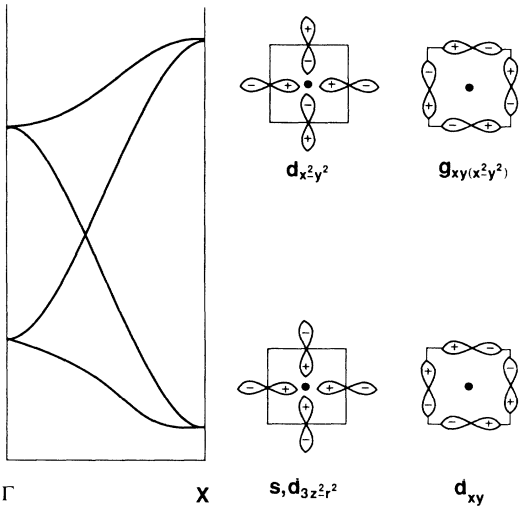


FIG. 2. Near-neighbor tight-binding $p$ bands for two-dimensional square O lattice. Sketches of $X$-point orbitals are labeled according to symmetry about the Cu sites at the center of the squares.

TABLE II. Summary of parameters calculated for the effective Hamiltonian, Eq. (4), of $La_2CuO_4$. Slater-Koster parameters $V$ describing the O($2p$)-O($2p$) and O($2p$)-Cu($3d$) hybridization, and band centers $C$ were obtained from analysis of the LMTO band structure for which Cu($3d$), $O_I(2p)$, and $O_{II}(2p)$ occupations were 9.45, 4.27, and 4.14, respectively. On-site Cu($3d$) and $O_I(2p)$, and near-neighbor Cu($3d$)-$O_I(2p)$ Coulomb interactions $U_d$, $U_p$, and $U_{pd}$ were obtained from LMTO constrained-occupation total-energy calculations, as was the Cu($3d$) electron addition energy $\varepsilon_d(d^{9.5})$, to be compared to the top of the O($2p$) band at $-2.6$ eV. All values here are in eV and were obtained using the sphere configurations of Table I.

| Band structure | | Total energy | |
|---|---|---|---|
| $V_{pp\sigma}$ | 1.0 | $U_d$ | 8.5 |
| $V_{pp\pi}$ | −0.3 | $U_p$ | 4.1–7.3 |
| $V_{pd\sigma}$ | −1.85 | $U_{pd}$ | 0.6–1.3 |
| $V_{pd\pi}$ | 0.75 | | |
| $C_d$ | −4.1 | $\varepsilon_d(d^{9.5})$ | −3.0 |
| $C_{Ip}$ | −5.3 | | |
| $C_{IIp}$ | −3.5 | | |

from the fit

$$E(n) = \text{const} + \varepsilon_0 n + \tfrac{1}{2} U n(n-1) + O(n^3) \qquad (1)$$

or equivalently from the self-consistent one-electron eigenvalues

$$\varepsilon(n) = \frac{\partial E(N)}{\partial n} = \varepsilon_0 + U(n - \tfrac{1}{2}) + O(n^2) . \qquad (2)$$

In the solid this procedure allows all the other electrons to readjust, and so yields an effective $U$ which includes screening by other electrons.

An indication of the reliability of local-density total-energy calculations of Coulomb interactions is provided by the isolated atom or ion limit, where comparison may be made to spectroscopic data. Table III makes such a comparison for Cu and O ions of varying $3d^n4s^m$ and $2p^n3s^m$ configurations, respectively. The experimental results are based on averages over all multiplets comprising each given configuration.[60] The first entry for each element is a one-particle level separation, e.g., the cost in energy $\underline{\varepsilon_d} - \underline{\varepsilon_s}$ to move the hole (denoted by the bar under $\underline{\varepsilon}$) from the $4s$ to the $3d$ shell in Cu. Subsequent entries are intra-atomic Coulomb repulsion energies $U$, both "bare" quantities $U^{(0)}$ appropriate to isolated atoms or ions, and "screened" values $U$ obtained from configurations where electrons are promoted keeping the total charge fixed. Theory and experiment differ in Table III by less than 1 eV, an uncertainty which we may anticipate in the solid as well. Furthermore, following the success of Herbst, Watson, and Wilkins[61] in applying similar screened $U_f$'s to rare-earth metals, we might guess $U$'s for a poor metal like $La_2CuO_4$ to be intermediate between the $U$ and $U^{(0)}$ values in Table III, e.g., $4 < U_d < 16$ eV.

Turning to the case of the solid, one would ideally like total-energy differences for the addition of electrons to a *single* Cu or O "impurity" site in the infinite crystal. The results reported here, however, are from superlattice calculations, in which the impurity site is repeated periodi-

TABLE III. Comparison with experiment of local density approximation (LDA) calculated constrained-occupation quantities for isolated Cu $3d^n4s^m$ and O $2p^n3s^m$ ions. All quantities are in eV.

| Quantity | Definition | LDA[a] | Expt[b] |
|---|---|---|---|
| | Cu | | |
| $\varepsilon_d-\varepsilon_s$ | $E(d^9s^2)-E(d^{10}s^1)$ | 2.03 | 1.49 |
| $U_s^{(0)}$ | $E(d^9s^2)+E(d^9s^0)-2E(d^9s^1)$ | 8.34 | 8.32 |
| $U_{sd}^{(0)}$ | $E(d^9s^0)-E(d^9s^1)-E(d^{10}s^0)+E(d^{10}s^1)$ | 9.81 | 9.75 |
| $U_d^{(0)}$ | $E(d^{10}s^1)+E(d^8s^1)-2E(d^9s^1)$ | 15.88 | 16.13 |
| $U_d$ | $E(d^{10}s^0)+E(d^8s^2)-2E(d^9s^1)$ | 3.96[c] | 4.36 |
| | O | | |
| | $E(p^3s^1)-E(p^4s^0)$ | 12.34 | 11.46 |
| $U_s^{(0)}$ | $E(p^2s^2)+E(p^2s^0)-2E(p^2s^1)$ | 5.48 | |
| $U_{sp}^{(0)}$ | $E(p^2s^0)-E(p^2s^1)-E(p^3s^0)+E(p^3s^1)$ | 7.64 | 7.67 |
| $U_p^{(0)}$ | $E(p^4s^0)+E(p^2s^0)-2E(p^3s^0)$ | 17.15 | 17.35 |
| $U_p$ | $E(p^4s^0)+E(p^2s^2)-2E(p^3s^1)$ | 7.35 | |

[a]The Cu (O) calculations were scalar (non) relativistic. Both used the exchange-correlation potential of von Barth and Hedin, Ref. 57.

[b]Reference 60; the average (e.g., over all 90 states for $d^8s^1$) energy has been used for each configuration.

[c]The LDA result for the corresponding neutral configurations $3d^{10-n}4s^n4p^1$ is 3.90 eV.

cally throughout the solid. There is no Coulomb divergence when the net charges of the spheres comprising the cell do not sum to zero, as the usual form of the LMTO intersphere Madelung energy includes a uniform neutralizing background.[54,55] However, it is necessary to demonstrate convergence of these results as a function of impurity separation in order to deduce a result appropriate to an isolated impurity. The smallest superlattice is taken here to be the bct structure of Table I, so that all Cu's or all $O_I$'s are affected. The impurity separation is then increased by a factor of $\sqrt{2}$, so that only half of the Cu's or $O_I$'s in each $CuO_2$ layer are affected. The resultant modest changes in $U$ suggest these calculations are sufficient.

There is no unique definition for the localized Cu($3d$) or O($2p$) Wannier functions which should be used for the constrained occupation calculations. This is less of a problem in the former case, as may be seen by analyzing the 5 "hybridized" Cu($3d$) bands obtained by excluding only $p$ character in the O spheres. Nearly all (97%) of the resultant state density arises from atomiclike $3d$ orbitals in the Cu spheres. By contrast, only 75% of the state density associated with the equivalent $O_I(2p)$ bands arises from $2p$ orbitals in the $O_I$ spheres (69% for $O_{II}$). Thus while O($2p$) Wannier functions will require significant amplitude in neighboring spheres (especially La), it is not unreasonable to approximate the Cu($3d$) Wannier functions by atomiclike $3d$ states entirely within the Cu spheres. The boundary condition which most naturally simulates a decaying tail is the band-center logarithmic derivative $-l-1=-3$, and more important, it yields an orbital energy within the 0.3-eV-wide unhybridized Cu-$3d$ band.

Self-consistent LMTO total-energy $E$ calculations were carried out with constrained Cu($3d$) impurity-site occupations $n$, for which the transition-state expression

$$E(d^{n+1})-E(d^n)\simeq\tfrac{1}{2}[\varepsilon_d(d^{n+1})+\varepsilon_d(d^n)]\simeq\varepsilon_d(d^{n+1/2}) \quad (3)$$

was generally valid to within 5% or better. We shall consider these three expressions as interchangeable; however, the eigenvalues $\varepsilon$ may be calculated with greater precision than the total energy, and were generally used for the results reported here. The important energies for the present application are those to add the ninth and tenth $3d$ electrons to the Cu impurity sites, so that in Table IV we report $\varepsilon_d(d^{9.5})$ and define $U_d$ as the difference between this value and $\varepsilon_d(d^{8.5})$.

The first block of three entries in Table IV shows the sensitivity of $\varepsilon_d(d^{9.5})$ and $U_d$ to the choice of $l_{\max}$ in the La and O (also empty) spheres. For the Cu spheres, $l_{\max}$ was $p$ for the impurity sites with constrained occupations, and otherwise $d$. $N_{\rm val}$ is the number of bandlike valence electrons per primitive cell, including La($5p$) and O($2s$). For bct lattice 1 (all Cu's affected) the choice $N_{\rm val}=44$, for example, leads to a net cell charge of 0.5, 0, and $-0.5$ for impurity occupations $n=8.5$, 9, and 9.5, respectively. Recall that we may reply on the intersphere Madelung term to provide a uniform background for the necessary charge compensation. Alternatively, one could change $N_{\rm val}$ (=variable in Table IV) for each $n$ to provide a neutral cell, which in effect transfers electrons between the impurity states and the band Fermi level. For larger supercells, these different choices for $N_{\rm val}$ become unimportant, as is readily evident by comparison of the second (20% variations in $U_d$) and third (5% variations) blocks of three lines each in Table IV. The impurity separation is increased by a factor of $\sqrt{2}$ in the case of lattice 2, which

TABLE IV. Cu($3d$) constrained-occupation calculations for $La_2CuO_4$. For lattice 1 (2), the $3d$ states of all (half) of the Cu's in each $CuO_2$ layer were treated in an atomic mode with constrained occupations. $R_{Cu}$ is the radius of the Cu spheres in bohrs. The $N_{val}$ valence electrons were sampled with $N_{IW}$ points per irreducible wedge, with maximum angular momentum $l_{max}$ in the La and O (also empty) spheres, respectively. The quantities $\varepsilon_d(d^{9.5})$ and $U_d=\varepsilon_d(d^{9.5})-\varepsilon_d(d^{8.5})$ are in eV. Values in parentheses signify use of the combined correction.

| Lattice | $R_{Cu}$ | $N_{val}$ | $N_{IW}$ | $l_{max}$ | $\varepsilon_d(d^{9.5})$ | $U_d$ |
|---|---|---|---|---|---|---|
| 1 | 2.48 | 44 | 18 | $dp$ | −2.00 | 7.78 |
| | | | | $fp$ | −2.91 | 7.85 |
| | | | | $fd$ | −3.03 | 7.88 |
| 1 | 2.48 | 44 | 18,75 | $dp$ | −2.00 | 7.78 |
| | | 43 | | | −1.22 | 7.44 |
| | | Variable | | | −2.57 | 9.02 |
| 2 | 2.48 | 97 | 27 | $dp$ | −2.27 | 8.30 |
| | | 96 | | | −1.96 | 8.23 |
| | | Variable | | | −2.11 | 8.63 |
| 1 | 2.48 | 44 | 18 | $dp$ | (−1.78) | (7.74) |
| | 2.728 | | | | (−2.37) | (7.17) |
| | 2.976 | | | | (−2.72) | (6.76) |

is treated as base-centered orthorhombic ($a'=\sqrt{2}a$, $b'=c$, $c'=\sqrt{2}a$) with two inequivalent Cu sites in each $CuO_2$ layer.

We consider $\varepsilon_d(d^{9.5})=-3\pm1$ and $U_d=8.5\pm1$ eV to be the converged values from Table IV, for a Cu sphere radius of $R_{Cu}=2.48$ bohrs, with the $\pm1$ eV uncertainty acknowledging in part the theory-experiment comparison for the isolated ion case of Table III. The $\varepsilon_d(d^{9.5})$ value anticipates $\approx1$ eV lowering of the results for lattice 2 with increased $l_{max}$, and is to be compared to the −2.6-eV position of the top of the O($2p$) bands in Fig. 1(b).

The last three entries in Table IV show the effects of 10% increases in the Cu sphere radius. Using the differences between these entries, we estimate converged values of $\varepsilon_d(d^{9.5})$ and $U_d$ for $R_{Cu}=2.728$ bohrs to be about −3.6 and 7.9 eV, respectively, to be compared with −3.0 and 8.5 eV, respectively, for $R_{Cu}=2.48$ bohrs. We do not consider this dependence on $R_{Cu}$ itself to be a convergence effect, but rather a redefinition of the Cu($3d$) Wannier function which must be accompanied by corresponding changes in the hybridization to be discussed shortly. Because of this interdependence it may not be fruitful to compare the value $U_d\approx8.5$ eV found here with, for example, values near 6 eV extracted from x-ray photoemission spectroscopy.[49–53] The comparison should come rather with results of the complete model calculations. The Cu radius in Table I was chosen to provide minimal overlap of the various spheres comprising the primitive cell, and thus improved accuracy of the LMTO method. Evidence of this is provided by the combined correction[54,55] which seeks to correct for sphere-polyhedra differences. While the effects on $U_d$ are small, its inclusion in the quantities in parentheses in Table IV has increased $\varepsilon_d(d^{9.5})$ by 0.22, 0.51, and 1.08 eV for $R_{Cu}=2.48$, 2.728, and 2.976 bohrs, respectively.

Before leaving the Cu($3d$) case, we comment on an alternate method of calculating $\varepsilon_d(d^n)$ due to Dederichs, Blügel, Zeller, and Akai[62] Figure 3 compares curves $\varepsilon_d(d^n)$ from our calculations described above with additional calculations that we have carried out using this other method. The solid and short-dashed curves in the figure show graphically the results given in the second line of Table IV with $N_{val}=44$, and the equivalent neutral-cell calculation with variable $N_{val}$. In both cases the impurity state is an atomiclike Cu($3d$) orbital decoupled from all other spheres and angular momentum components. The comparison long-dashed curve in Fig. 3 was obtained by the method of Dederichs *et al.*,[62] in which all Cu($3d$) states are fully hybridized as in Fig. 1(a). In this method one varies $\varepsilon_d$ and calculates the change in occupation. Here $n$ represents the integrated $d$-state density within the Cu impurity sphere, which is altered by shifting the $l=d$ potential in these spheres by $-\varepsilon_d$, the independent variable in this approach. While the slope of the long-dashed curve approaches the other two for smaller $n$, the upward bend as $n$ approaches 10 yields an unreasonable $U_d=\varepsilon_d(d^{9.5})-\varepsilon_d(d^{8.5})\approx24$ eV. This behavior arises from the effects of hybridization, which will always put some $d$ state density above the Fermi level of a metal as in Fig. 1(a), making it difficult to achieve $n=10$. This simple hybridization effect must be removed from the calculation in order to extract the true interactions.

We now consider constrained occupation calculations for the O($2p$) states with the results in Table V. Given the more extended nature of the O($2p$) Wannier states, the present treatment which considers only atomiclike $2p$

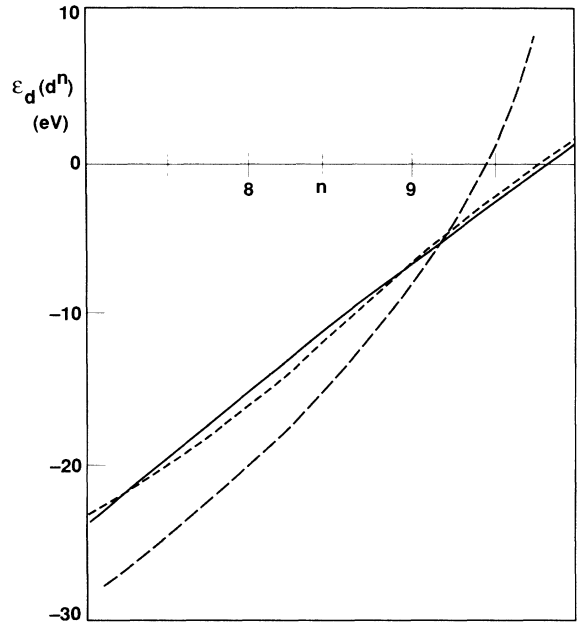


FIG. 3. Cu($3d$) orbital energy $\varepsilon_d(d^n)$ as a function of occupation $n$. Constrained occupation calculations with fixed and variable number of valence electrons are given by the solid and short-dashed curves, respectively. The long-dashed curve was obtained using the method of Dederichs *et al.* (Ref. 62). All three calculations were for the smallest superlattice, the bct structure itself.

TABLE V. O(2$p$) constrained-occupation calculations for $La_2CuO_4$. Configurations $d^n p^m$ refer to atomiclike treatment of Cu(3$d$) and $O_I$(2$p$) states with occupations $n$ and $m$, respectively. Both (half) of the $O_I$'s were affected for lattice 1 (2). $N_{val}$ is the number of electrons per primitive cell treated in a band mode. The irreducible wedges were sampled with 18 and 27 points, respectively, with $d$ (La) and $p$ (O, empty spheres) maximum angular momenta used for sites with unconstrained occupations. Values in parentheses are normalized to account for the extended wave functions as discussed in the text. Calculated values are in eV.

| Quantity | Definition | Lattice | $N_{val}$ | Value |
|---|---|---|---|---|
| $U_p$ | $\varepsilon_p(p^{5.5})-\varepsilon_p(p^{4.5})$ | 1 | 41 | 7.16 (4.0) |
| | | 2 | 47 | 7.29 (4.1) |
| $U_{pd}$ | $\frac{1}{4}[\varepsilon_d(d^{9.5}p^{5.5})-\varepsilon_d(d^{9.5}p^{4.5})]$ | 1 | 32 | 0.82 (1.5) |
| | $\frac{1}{2}[\varepsilon_d(d^{9.5}p^{5.5})-\varepsilon_d(d^{9.5}p^{4.5})]$ | 2 | 38 | 0.63 (1.3) |
| $U_{pd}$ | $\frac{1}{2}[\varepsilon_p(d^{9.5}p^{5.5})-\varepsilon_p(d^{8.5}p^{5.5})]$ | 1 | 32 | 0.93 (1.6) |
| | $\frac{1}{2}[\varepsilon_p(d^{9.5}p^{5.5})-\varepsilon_p(d^{8.5}p^{5.5})]$ | 2 | 38 | 0.61 (1.3) |

orbitals within the O spheres is more tenous than for the Cu(3$d$) case. We can find an upper bound for $U_p$ by changing the charge in the O spheres by unity, and using the band-center logarithmic derivative $l-1=-2$ to specify the impurity O(2$p$) eigenvalue. The first two lines of Table V show rapid convergence with impurity separation, yielding $U_p \approx 7$ eV. All $O_I$ atoms were affected for bct lattice 1; only half in each $CuO_2$ layer, for lattice 2. The latter was treated as body-centered orthorhombic in order to insure the right irreducible wedge while treating the two $O_I$ sites as inequivalent. Since only 75% of the $O_I$(2$p$) Wannier function $|\phi_p|^2$ lies within the $O_I$ sphere, and our designation $p^n$ refers only to occupation of this sphere, we might estimate the addition energy of the sixth $O_I$(2$p$) electron from $E(p^{6x})-E(p^{5x})=x\varepsilon_p(p^{5.5x})$, where $x=0.75$. Such logic leads also to values of $U$ scaled by $x^2$, i.e., $U_p=(7.3\text{ eV})\times(0.75)^2=4.1$ eV which is a reasonable lower bound and is given in parentheses in Table V.

By constraining both Cu(3$d$) and O(2$p$) occupations for a combined set of impurity sites, one may also estimate $U_{pd}$, the additional energy cost to add a 3$d$ hole to a Cu site in the presence of a 2$p$ hole on a neighboring O site, or vice versa. For the larger impurity separation we obtain $U_{pd}=0.6$ eV in Table V, which we view as a slight underestimate since our calculations omit tails of the O(2$p$) Wannier function which extend into the Cu spheres (about 8%). Thus an upperbound might be 0.6 eV $+0.08U_d=1.3$ eV as indicated in parentheses in Table V. We note that Chen, Wang, Leung, and Harmon[47] report $U_{pd}=1.6$ eV along with $U_p=14.3$ eV. Their calculations are tight-binding fits which are in some ways similar in spirit to the present work. But they made an assumption that $e_d^o-e_p^o=0$, where $e_d^o$ and $e_p^o$ are the Cu $d_{x^2-y^2}$ and $O_I$ $p_{x,y}$ orbital energies *in the presence of two holes each.* However, the value we find for $\varepsilon_d(d^8p^4)-\varepsilon_p(d^8p^4)$ is $e_d^o-e_p^o\approx -7$ eV. From preliminary work, we believe that this change in energies would shift their values to $U_{pd}=0.9$ eV and $U_p=8.7$ eV in better agreement with ours.

### C. Effective electronic Hamiltonian

We now summarize the results of Secs. II A and II B in the form of an effective Hamiltonian in a site basis. Let $p_{i\mu}^\dagger$ be the operator that creates a *p hole* on O site $i$ of type $\mu$ ($p_{x\uparrow}$, $p_{y\uparrow}$, etc.) and $d_{jv}^\dagger$ the creation operator for a *d hole* on Cu site $j$ of type $v$ ($d_{x^2-y^2\uparrow}$, etc.). Considering near-neighbor $O_I$-$O_I$, $O_I$-$O_{II}$, and $O_{II}$-$O_{II}$ pairs $\langle i,i'\rangle$, in addition to $O_I$-Cu and $O_{II}$-Cu pairs $\langle i,j\rangle$, the effective Hamiltonian may be written

$$H=\underline{\varepsilon}_{Ip}\sum_{i,\mu}^{I} p_{i\mu}^\dagger p_{i\mu}+\underline{\varepsilon}_{IIp}\sum_{i}^{II} p_{i\mu}^\dagger p_{i\mu}+U_p\sum_{\substack{i,\mu,\mu'\\ \mu<\mu'}} n_{i\mu}n_{i\mu'}+\underline{\varepsilon}_d\sum_{jv} d_{jv}^\dagger d_{jv}+U_d\sum_{\substack{j,v,v'\\ v<v'}} n_{jv}n_{jv'}$$
$$+\sum_{\langle i,i'\rangle,\mu,\mu'} V_{i\mu,i'\mu'}(p_{i\mu}^\dagger p_{i'\mu'}+\text{H.c.})+\sum_{\langle i,j\rangle,\mu,v} V_{i\mu,jv}(p_{i\mu}^\dagger d_{jv}+\text{H.c.})+U_{pd}\sum_{\langle i,j\rangle,\mu,v} n_{i\mu}n_{jv}. \tag{4}$$

A tabulation of our calculated values for these parameters is given in Table II. We expect the band centers $C$ to give reasonable estimates of the relative hole energies $\underline{\varepsilon}$ i.e., $\underline{\varepsilon}_{Ip}-\underline{\varepsilon}_d=-C_{Ip}+C_d=1.2$ eV, and similarly for the $O_{II}$ case. A single energy $\underline{\varepsilon}_d$ will suffice, as we argue in Appendix A that point-charge crystal-field splitting of the Cu(3$d$) level is negligible for our choice of basis. The Coulomb interactions which we have considered are $U_p$ and $U_d$ for any two holes on the same O or Cu sites, and $U_{pd}$ for holes on neighboring O and Cu sites. We apply the values in Table II for $U_p$ and $U_{pd}$ estimated for $O_I$ holes to $O_{II}$ holes as well.

The hybridization matrix elements $V_{i\mu,i'\mu'}$ and $V_{i\mu,jv}$ must be evaluated in terms of the $\sigma$ and $\pi$ Slater-Koster parameters (e.g., $V_{pp\sigma}$) given in Table II, and the direction cosines between the sites $i$ and $i'$ (or $j$), according to the expressions in Ref. 59. The matrix element $V_{i\mu,jv}$ between a $d_{x^2-y^2}$ Cu orbital and a neighboring $O_I$ $p_\sigma$ orbital (i.e., pointed toward the Cu site), often termed $t_{pd}$, is $t_{pd}=(\sqrt{3}/2)V_{pd\sigma}=-1.6$ eV. This is the single parameter in the simplest tight-binding model and our value should be identical to that of Mattheiss,[31] as he quotes the same $-1.85$-eV value for the Slater-Koster parameter. The matrix element between near-neighbor $O_I$ $p_\sigma$ states

(which point towards their common near-neighbor Cu site) is $t_{pp}=\frac{1}{2}(V_{pp\sigma}-V_{pp\pi})=0.65$ eV, which may be compared to the value $\approx 0.5$ cited by Weber[26] and $\approx 0.6$ by Stechel and Jennison.[27]

The $O_I(2p)$-$O_I(2p)$ Slater-Koster parameters in Table II may be extended to near-neighbor $O_I$-$O_{II}$ and $O_{II}$-$O_{II}$ pairs using $d^{-l-l'-1}=d^{-3}$ scaling. Taking relative band centers $C_{Ip}$ and $C_{IIp}$, they produce combined O bands for the $La_2CuO_4$ structure of 6.5 eV width and a similar overall flatness at the top as seen in Fig. 1(b). Note that the corresponding two-dimensional $O_I(2p)$ bandwidth $8t_{pp}=4(V_{pp\sigma}-V_{pp\pi})=5.2$ eV is smaller. While most models for $La_2CuO_4$ ignore the O bandwidth, recent papers have acknowledged its importance.[17,18,26,27] Newns and co-workers[17,18] and Weber[26] cite widths $\approx 4$ eV which we believe should be compared to our 5.2-eV $O_I$ width. We believe this difference reflects the choice of basis, specifically that our Cu($3d$) Wannier function is defined to exist only within the Cu atomic spheres, and that the O band in Fig. 1(b) is hybridized with all components except this Cu($3d$) orbital. We emphasize that the parameters in Table II are internally consistent, and that the ambiguity in choice of basis offers flexibility which may be used to simplify solution of the problem.

The Hamiltonian Eq. (4) is still very complex because it involves so many bands. We believe our work indicates that $U_{pd}$ is sufficiently small that it should not have qualitative effects. Such an interaction has been studied in model simulations by Hirsch and co-workers[21,22] and Schüttler[23] and in theories based upon exciton mechanisms of superconductivity.[20] Our value of $U_{pd}/t_{pd}\leq 0.8$ is smaller than values $\geq 2$–$4$ which were found by Hirsch and co-workers[21,22] to lead to a superconducting ground state in Monte Carlo simulations. In addition, we propose that as a first approximation $U_p$ can be ignored. The rationale is that the large bandwidth of the O electrons (6.7 eV), which is comparable to or larger than $U_p$ (4.1–7.3 eV), causes the electrons to act as bandlike in the O states. This is very similar to the reasoning used in heavy-fermion systems.

If both $U_p$ and $U_{pd}$ are ignored, then the Hamiltonian equation (4) reduces to a degenerate Anderson lattice model similar to ones used to describe heavy-fermion and mixed-valence systems. This is still complex because so many bands are involved. Our results suggest that the bands which are potentially relevant for excitations near the Fermi energy are (1) the $d_{x^2-y^2}$ Cu states mixed with O; (2) $d_{3z^2-r^2}$ states mixed with O; and (3) one or more of the uppermost O bands in Fig. 1(b) which do not couple or are weakly coupled to Cu. We note that recent papers by Goddard and co-workers[15] and Birgeneau, Kastner, and Aharony[16] have proposed that holes go into $O_I$ $p_\pi$ states, which have the same form as the $g_{xy(x^2-y^2)}$ O molecular orbital in Fig. 2. Since such states are near the top of our O bands, we believe this to be a possibility.

### D. Hybridization in the impurity Anderson model

The hybridization between an impurity Cu($3d$) level and a band of itinerant O($2p$) states may be obtained from the approximate parameters in Table II. However, more accurate calculation of these functions is possible using other techniques, which we now review. In order to generate a hybridization matrix consistent with that appearing in the Anderson Hamiltonian, it is necessary to be able to write the matrix $H$ which generates the LMTO one-electron eigenvalues at a particular $\mathbf{k}$ point in the form:

$$H=H^{(0)}+V=\begin{pmatrix}H_{11}^{(0)} & 0\\ 0 & H_{22}^{(0)}\end{pmatrix}+\begin{pmatrix}0 & V_{12}\\ V_{21} & 0\end{pmatrix}, \tag{5}$$

where the index 1 ranges over the impurity Cu($3d$) states; and 2, all other states. It is presumed that $H_{11}^{(0)}$ should generate a *narrow,* unhybridized Cu($3d$) band, and that the hybridization $V$ has no diagonal, e.g., $V_{22}$ elements. Furthermore, internal consistency between the calculations of $U_d$ and the hybridization require that the states used in the constrained occupation calculations should also be those which define the matrix elements of $H_{11}^{(0)}$ and $V_{12}$.

Equation (5) is easily satisfied in the newer orthogonal basis representation of the LMTO method.[56] For the original formulation which has significant overlap matrices, an approximation to the desired matrix $V$ may be generated in the manner we have reported previously for the rare-earth dioxides.[43] In this approach, $H^{(0)}$ is defined by removing all coupling between Cu($3d$) and other states in the structure constant matrix. While the resultant $\Delta H\equiv H-H^{(0)}$ has the undesired property $\Delta H_{22}\neq 0$, a perturbation treatment was used to derive an analytic expression for an effective $V_{12}$, linear in the structure constant matrices, which satisfies Eq. (5) to a good approximation. This approach has been used for the symmetry decomposed hybridization functions $|V_\mu(\varepsilon)|^2$ in the present work, and it is consistent with our $U_d$ calculation. The two methods should be nearly equivalent, and test comparisons have been found to yield the same area under the symmetry-averaged $|V(\varepsilon)|^2$ to within 7%.

Since the unhybridized Cu($3d$) band is quite narrow, one may approximate the weakly $\mathbf{k}$-dependent matrix $H_{11}^{(0)}$ at each point in the Brillouin zone by a $\mathbf{k}$-independent matrix with eigenvectors appropriate to a local, one-electron $d$ state in a tetragonal environment. After a unitary transformation which diagonalizes the modified $H^{(0)}$, the hybridization matrix elements become $V_{\mu j,\mathbf{k}i}$, and

$$|V_\mu(\varepsilon)|^2=\frac{1}{\Omega_0}\int_{BZ}d\mathbf{k}\sum_i\delta(\varepsilon-\varepsilon_{\mathbf{k}i})\,|V_{\mu j,\mathbf{k}i}|^2. \tag{6}$$

Here the $\varepsilon_{\mathbf{k}i}$ are the eigenvalues of $H_{22}^{(0)}$ corresponding to the O($2p$) band in Fig. 1(b), indexed by $\mathbf{k}$-vector and band index $i$, while $\mu$ and $j$ are the irreducible representation and partner for the Cu($3d$) impurity site, respectively. The integral is over the first Brillouin zone (BZ) of volume $\Omega_0$.

We have calculated $|V_\mu(\varepsilon)|^2$ using the smallest supercell, i.e., the bct structure itself. The irreducible wedge of the Brillouin zone was sampled with 75 points, and the tetrahedral method was then used to evaluate Eq. (6).

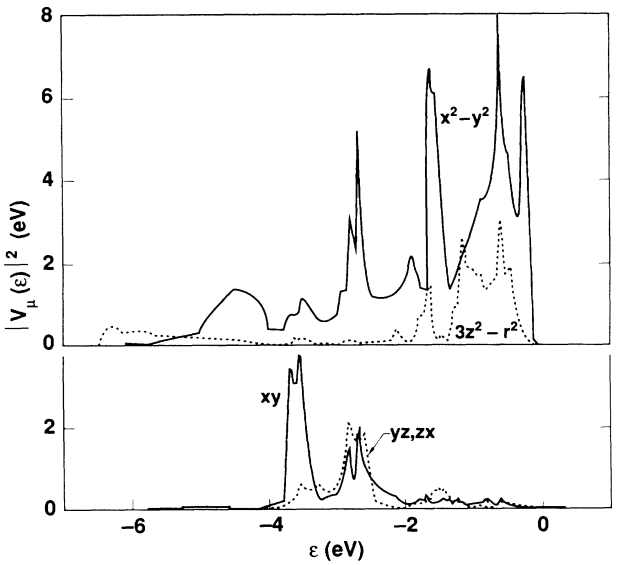


FIG. 4. Calculated hybridization functions $|V_\mu(\varepsilon)|^2$ between a local Cu($3d$) level and itinerant O($2p$) bands in $La_2CuO_4$.

The results for $|V_\mu(\varepsilon)|^2$ are shown in Fig. 4, obtained using a 2.48-bohrs Cu-sphere radius. The integrated areas under these curves are 10.3 $eV^2$ ($\Gamma_3 = x^2-y^2$), 2.7 $eV^2$ ($\Gamma_1 = 3z^2-r^2$), 2.3 $eV^2$ ($\Gamma_4 = xy$), and 1.4 $eV^2$ ($\Gamma_5 = yz,zx$). If the radius of the Cu sphere is increased to 2.728 bohrs, and the other spheres proportionally reduced, these areas decrease by 8.7%, 6.2%, 2.2%, and 1.4%, respectively. Note that the $x^2-y^2$ area is nearly four times larger than for any other symmetry, which should be no surprise given the emphasis placed on this coupling in tight-binding models. Equally important for the electronic states is the fact that the $x^2-y^2$ hybridization is also peaked up at the top of the O($2p$) band in Fig. 1(b). This follows from the fact already discussed that the O molecular orbital with $d_{x^2-y^2}$ symmetry about the Cu site is the O–O *antibonding* state sketched in Fig. 2. The $O_{II}$ contribution to the combined O($2p$) bands occurs mostly in the top third of the 6.7-eV range in Fig. 1(b), leading to the similar position of the $3z^2-r^2$ hybridization in Fig. 4. The symmetry-averaged $|V(\varepsilon)|^2$ is quite similar in shape to the O($2p$) density of states. The square root of its area and that for the dominant $x^2-y^2$ symmetry are 1.9 and 3.2 eV, respectively, which may be compared to the parameter $T = 2.3$ eV extracted by Shen *et al.*[50] from photoemission data.

Evaluation of Eq. (6) for the simple tight-binding model discussed in Sec. II A yields $3V_{pd\sigma}^2$ and $4V_{pd\pi}^2$ for the areas under the $x^2-y^2$ and $xy$ $|V_\mu(\varepsilon)|^2$ curves, and the areas just cited were in fact used to obtain the values of these two Slater-Koster parameters for Table II. Furthermore, $V_{pd\sigma}^2+2V_{pd\sigma}'^2$ and $2V_{pd\pi}^2+2V_{pd\pi}'^2$ should be the areas under the $3z^2-r^2$ and $yz,zx$ curves, where the $V'$'s are Cu-$O_{II}$ couplings. This suggests that the $3z^2-r^2$ area should be at least a third of the $x^2-y^2$ area, which it is not. Such a constraint is obeyed when the $|V_\mu(\varepsilon)|^2$ curves are calculated including only O $p$ components in the "O($2p$)" bands. However, especially the admixture of La character and Cu $s$ character into these bands significantly reduces the $3z^2-r^2$ area. This behavior points to possible limitations of any simple tight-binding parametrization as set out in Sec. II A.

## III. IMPURITY ANDERSON MODEL FOR $La_2CuO_4$

The results of Sec. II suggest that an Anderson model is appropriate for the Cu-O based systems. In this section we consider the impurity limit of this Hamiltonian since it can be solved exactly for the ground-state energy and spectra. We have solved the impurity Anderson model for a local Cu($3d$) level embedded in the continuum provided by the predominantly oxygen bands, using the parameters of Sec. II. The dominant $x^2-y^2$ hybridization leads to a magnetic ground state with spin $\frac{1}{2}$ and $d_{x^2-y^2}$ orbital symmetry, and of central importance to this paper, it pushes a sharp level in the electron removal spectrum above the top of the full O($2p$) band. The two holes in this *singlet* ground state of the $(N-1)$-electron system are highly correlated, having little probability of both being on the Cu impurity site. We argue on the basis of cluster calculations in Appendix B that the qualitative nature of this state is unchanged by inclusion of our estimates for $U_p$ and $U_{pd}$. Within the uncertainties in our parameters, we find reasonable agreement between our calculated $d$-spectral weight for electron removal and the photoemission data for $La_2CuO_4$.

We write the Hamiltonian Eq. (4) for the impurity-model calculations in the form

$$H=\sum_{\nu,\tau}\left(\int_0^B d\varepsilon\,\varepsilon\psi_{\varepsilon\nu\tau}^\dagger\psi_{\varepsilon\nu\tau}+\underline{\varepsilon}_d\psi_{\nu\tau}^\dagger\psi_{\nu\tau}\right)+U_d\sum_{\substack{\mu,\sigma,\nu,\tau\\ \mu,\sigma<\nu,\tau}}n_{\mu\sigma}n_{\nu\tau}+\sum_{\nu,\tau}\int_0^B d\varepsilon[V_\nu(-\varepsilon)\psi_{\nu\tau}^\dagger\psi_{\varepsilon\nu\tau}+\text{H.c.}]\,, \tag{7}$$

where $\psi_{\varepsilon\nu\tau}^\dagger$ creates a *hole* of energy $\epsilon$ in the O($2p$) states, and $\psi_{\nu\tau}^\dagger$ creates a *hole* of energy $\underline{\varepsilon}_d$ on the impurity level. A single $\underline{\varepsilon}_d$ is adequate, as we find point-charge crystal-field and spin-orbit effects to be small (see Appendix A). The indices $\mu$ and $\nu$ cover symmetry (and partner in the case of $\Gamma_5 = yz,zx$), while $\sigma$ and $\tau$ designate spin. Taking the −2.6-eV top of the O($2p$) bands in Fig. 1(b) as the zero of energy, the hole energy $\underline{\varepsilon}_d = -\varepsilon_d(d^{9.5}) - 2.6$ eV, with $\varepsilon_d(d^{9.5})$ the quantity in Table II. Following Gunnarsson and Schönhammer, only those linear combinations of O($2p$) states (indexed by $\nu$) which can couple with the impurity level are included in the Hamiltonian.[40]

The O($2p$) bandwidth in Fig. 1(b) is $B=6.7$ eV, and so with our zero of energy O($2p$) holes are created over the range 0–6.7 eV.

### A. Ground state and electron addition spectrum

We consider the ground state $\Phi_{g\mu\sigma}^{(N)}$ of the $N$-electron system

$$\Phi_{g\mu\sigma}^{(N)}=A_\mu\left(|\mu\sigma\rangle+\int_0^B d\varepsilon a_\mu(\varepsilon)|\varepsilon\mu\sigma\rangle\right) \tag{8}$$

to be a linear combination of configurations $|\mu\sigma\rangle \equiv\psi_{\mu\sigma}^\dagger|0\rangle$ with one hole on the impurity site, and $|\varepsilon\mu\sigma\rangle\equiv\psi_{\varepsilon\mu\sigma}^\dagger|0\rangle$ with one hole in the O bands. As long as we preclude electron excitations into the La($4f$,$5d$) conduction bands above the gap in Fig. 1(b), the number of possible configurations both here and for the $(N-1)$-electron system are limited, so that essentially an exact solution of Eq. (7) is possible without resorting to $1/N$ expansions. Considering the vacuum $|0\rangle$, energy $E_0$ (subsequently taken to be 0), to correspond to fully occupied impurity states and O bands, then the ground-state energy $E_{g\mu}^{(N)}$ and wave functions are given by

$$E_{g\mu}^{(N)}\equiv E_0+\Delta E_\mu\,, \tag{9}$$

$$\Delta E_\mu=\underline{\varepsilon_d}+\int_0^B d\varepsilon\frac{|V_\mu(-\varepsilon)|^2}{\Delta E_\mu-\varepsilon}\,, \tag{10}$$

$$a_\mu(\varepsilon)=\frac{V_\mu^*(-\varepsilon)}{\Delta E_\mu-\varepsilon}\,, \tag{11}$$

$$|A_\mu|^{-2}=1+\int_0^B d\varepsilon\frac{|V_\mu(-\varepsilon)|^2}{(\Delta E_\mu-\varepsilon)^2}\,. \tag{12}$$

The average number of $d$ *holes* occupying the impurity site is then

$$\langle N|\underline{n_d}|N\rangle=\langle\Phi_{g\mu\sigma}^{(N)}|\psi_{\mu\sigma}^\dagger\psi_{\mu\sigma}|\Phi_{g\mu\sigma}^{(N)}\rangle=|A_\mu|^2\,. \tag{13}$$

It is evident from Eqs. (9)–(12) that the ground-state energy depends on the symmetry of the hole in $\Phi_{g\mu\sigma}^{(N)}$. Table VI lists results for $\Delta E_\mu$ obtained with values of $\underline{\varepsilon_d}$, $U_d$, and $|V_\mu(\varepsilon)|^2$ determined in Sec. II. The first two cases use consistent theoretical values for LMTO Cu sphere radii of 2.48 and 2.728 bohrs, respectively. The last two will be discussed shortly. The ground state is clearly of $x^2-y^2$ symmetry, not surprising since the hybridization is so dramatically stronger in this case. The splittings between the $\Delta E_\mu$ are crystal field levels; in a similar calculation for $PrO_2$ we obtained the correct symmetries and first excitation interval to within 20% of that obtained by neutron scattering.[43] For $La_2CuO_4$, one may expect these levels to be significantly broadened by lattice effects. There are, however, indications in reflectivity[63,64] and photoluminescence[65] measurements on the CuO superconductors of weak absorption features in the 1–3 eV range, where Geserich *et al.*[63] identify as these $d$-$d$ transitions allowed by electric quadrupole selection rules.

The $d$-spectral weight for electron addition, to be compared to bremsstrahlung isochromat spectroscopy (BIS) experiments, is quite simple in the case of the $N$-electron ground state given by Eq. (8):

$$\rho^{\rm BIS}(E)=\frac{1}{\pi}{\rm Im}\left\langle\Phi_{g\mu\sigma}^{(N)}\middle|\psi_{\mu\sigma}^\dagger\frac{1}{E-i\eta+E_{g\mu}^{(N)}-H}\psi_{\mu\sigma}\middle|\Phi_{g\mu\sigma}^{(N)}\right\rangle \tag{14}$$

$$=|A_\mu|^2\delta(E+\Delta E_\mu)\,, \tag{15}$$

where $\eta$ in Eq. (14) is a positive infinitesimal. Clearly there is a contribution only for $\mu=x^2-y^2$, as an electron can be added to (hole destroyed in) the ground state only for this symmetry. The position of this (sharp, in the present model) peak is at $E_{\rm BIS}=-\Delta E_{x^2-y^2}$ relative to the top of the O($2p$) band, and is given in Table VI along with the weight $w_{\rm BIS}=|A_{x^2-y^2}|^2$ of the pole.

### B. Electron removal spectrum

The $d$-spectral weight for electron removal, to be compared to photoemission spectroscopy (PES) experiments, is given by

$$\rho^{\rm PES}(E)=\frac{1}{\pi}{\rm Im}\,g^<(E-i\eta)\,, \tag{16}$$

$$g^<(z)=\sum_{\nu,\tau}\left\langle\Phi_{g\mu\sigma}^{(N)}\middle|\psi_{\nu\tau}\frac{1}{z-E_{g\mu}^{(N)}+H}\psi_{\nu\tau}^\dagger\middle|\Phi_{g\mu\sigma}^{(N)}\right\rangle. \tag{17}$$

The results are conveniently expressed in terms of two defined functions:

$$f_\nu(\varepsilon',\varepsilon)\equiv[z-\Delta E_\mu+\varepsilon+\underline{\varepsilon_d}-\Gamma_\nu(z-\Delta E_\mu+\varepsilon)]\delta(\varepsilon'-\varepsilon)\,, \tag{18}$$

$$g_{\nu'\nu}(\varepsilon',\varepsilon)\equiv-\frac{V_{\nu'}^*(-\varepsilon')V_\nu(-\varepsilon)}{z-\Delta E_\mu+\varepsilon'+\varepsilon}\,, \tag{19}$$

where the dependence on $z$ and $\mu$ is not explicitly shown, and

$$\Gamma_\nu(z)\equiv\int_0^B d\varepsilon\frac{|V_\nu(-\varepsilon)|^2}{z+\varepsilon}\,. \tag{20}$$

Evaluation of the inverse $(z-E_{g\mu}^{(N)}+H)^{-1}$ requires separate treatment for $\mu\sigma=\nu\tau$ and $\mu\sigma\neq\nu\tau$. In the former case, we take as the $(N-1)$-electron basis for the inversion

$$|\mu\sigma,\varepsilon\mu\sigma\rangle\equiv\psi_{\mu\sigma}^\dagger\psi_{\varepsilon\mu\sigma}^\dagger|0\rangle\,, \tag{21a}$$

$$|\varepsilon'\mu\sigma,\varepsilon\mu\sigma\rangle\equiv\psi_{\varepsilon'\mu\sigma}^\dagger\psi_{\varepsilon\mu\sigma}^\dagger|0\rangle\,, \tag{21b}$$

where in Eq. (21b) $\varepsilon'>\varepsilon$. The resulting contribution to $g^<(z)$ is

$$g_{\nu\tau=\mu\sigma}^<(z)=|A_\mu|^2a_\mu^*(\varepsilon')[f_\mu(\varepsilon',\varepsilon)-g_{\mu\mu}(\varepsilon',\varepsilon)]^{-1}a_\mu(\varepsilon) \tag{22}$$

with the Einstein summation convention for the repeated indices $\varepsilon'$ and $\varepsilon$.

To carry out the inversion for the case $\nu\tau\neq\mu\sigma$, we take

TABLE VI. Impurity Anderson model calculations for $La_2CuO_4$. *N-electron (one hole) system:* Excited state $\Delta E_\mu$ and ground state $\Delta E_{x^2-y^2}$ energies, and the number of ground state $d$ holes $\langle N|\underline{n}_d|N\rangle$ are given. *(N−1)-electron (two-hole) ground state:* The probabilities of both holes being on impurity ($w_{dd}$) or O ($w_{pp}$) sites, or one on each ($w_{pd}$) are given along with the number of $d$ holes $\langle N-1|\underline{n}_d|N-1\rangle$. The first ionization energy is $E_{\rm PES}$ ($d$ spectral weight $w_{\rm PES}$). *(N+1)-electron ground state:* The first affinity level is $E_{\rm BIS}$ ($d$ spectral weight $w_{\rm BIS}$). The insulating gap is $E_{\rm gap}$. Values assumed for $\underline{\varepsilon}_d$ and $U_d$, and the radius $R_{\rm Cu}$ of the LMTO sphere used in obtaining the hybridization, are shown. All energies are in eV.

| Quantity | Case 1 | Case 2 | Case 3 | Case 4 |
|---|---|---|---|---|
| $\underline{\varepsilon}_d$ | 0.4 | 1.0 | −0.1 | −0.6 |
| $U_d$ | 8.5 | 7.9 | 6.5 | 7.5 |
| $R_{\rm Cu}$ | 2.48 | 2.728 | 2.48 | 2.48 |
| | | $N$-electron system | | |
| $\Delta E_{yz,zx}$ | −0.19 | 0.18 | −0.59 | −1.02 |
| $\Delta E_{xy}$ | −0.36 | 0.06 | −0.75 | −1.18 |
| $\Delta E_{3z^2-r^2}$ | −0.87 | −0.51 | −1.19 | −1.54 |
| $\Delta E_{x^2-y^2} = -E_{\rm BIS}$ | −2.32 | −1.84 | −2.61 | −2.92 |
| $\langle N|\underline{n}_d|N\rangle = w_{\rm BIS}$ | 0.56 | 0.51 | 0.60 | 0.64 |
| | | $(N-1)$-electron system | | |
| $w_{dd}$ | 0.06 | 0.05 | 0.10 | 0.10 |
| $w_{pp}$ | 0.36 | 0.40 | 0.30 | 0.28 |
| $w_{pd}$ | 0.58 | 0.55 | 0.60 | 0.62 |
| $\langle N-1|\underline{n}_d|N-1\rangle$ | 0.70 | 0.65 | 0.80 | 0.82 |
| $E_{\rm PES}$ | 1.05 | 0.88 | 1.29 | 1.29 |
| $w_{\rm PES}$ | 0.29 | 0.27 | 0.34 | 0.34 |
| $E_{\rm gap}$ | 1.27 | 0.96 | 1.32 | 1.63 |

the basis

$$|\nu\tau,\mu\sigma\rangle \equiv \psi^\dagger_{\nu\tau}\psi^\dagger_{\mu\sigma}|0\rangle\,, \tag{23a}$$

$$|\nu\tau,\varepsilon_1\mu\sigma\rangle \equiv \psi^\dagger_{\nu\tau}\psi^\dagger_{\varepsilon_1\mu\sigma}|0\rangle\,, \tag{23b}$$

$$|\varepsilon_2\nu\tau,\mu\sigma\rangle \equiv \psi^\dagger_{\varepsilon_2\nu\tau}\psi^\dagger_{\mu\sigma}|0\rangle\,, \tag{23c}$$

$$|\varepsilon_3\nu\tau,\varepsilon_4\mu\sigma\rangle \equiv \psi^\dagger_{\varepsilon_3\nu\tau}\psi^\dagger_{\varepsilon_4\mu\sigma}|0\rangle\,. \tag{23d}$$

The combined contributions to $g^<(z)$ from all eight values of $\nu\tau$ for which $\nu\neq\mu$ is

$$g^<_{\nu\neq\mu}(z) = |A_\mu|^2 \sum_{\substack{\nu \\ \nu\neq\mu}} N_\nu [1 \;\; a^*_\mu(\varepsilon_1') \;\; 0] G \begin{pmatrix} 1 \\ a_\mu(\varepsilon_1) \\ 0 \end{pmatrix}. \tag{24}$$

Here $N_\nu=2$ is the spin degeneracy, except for $N_{yz,zx}=4$, where we now restrict $\nu$ to just the four irreducible representations. The matrix $G$ is defined by its inverse

$$G^{-1} = \begin{pmatrix} z-\Delta E_\mu+2\underline{\varepsilon}_d+U_d & V_\mu(-\varepsilon_1) & V_\nu(-\varepsilon_2) \\ V^*_\mu(-\varepsilon_1') & f_\nu(\varepsilon_1',\varepsilon_1) & g_{\mu\nu}(\varepsilon_1',\varepsilon_2) \\ V^*_\nu(-\varepsilon_2') & g_{\mu\nu}(\varepsilon_2',\varepsilon_1) & f_\mu(\varepsilon_2',\varepsilon_2) \end{pmatrix}. \tag{25}$$

The zeros in the row and column vectors in Eq. (24) correspond to $\varepsilon_2'$ and $\varepsilon_2$, respectively, and integration over the range 0 to $B$ for all of $\varepsilon_1'$, $\varepsilon_2'$, $\varepsilon_1$, and $\varepsilon_2$ is intended in Eq. (24).

The case where $\nu=\mu$ and $\tau\neq\sigma$ further simplifies and may be combined with Eq. (22) to yield

$$g^<_{\nu=\mu}(z) = \tfrac{1}{2}|A_\mu|^2(N_\mu-1)[\sqrt{2}\,a^*_\mu(\varepsilon')] \begin{pmatrix} z-\Delta E_\mu+2\underline{\varepsilon}_d+U_d & \sqrt{2}V_\mu(-\varepsilon) \\ \sqrt{2}V^*_\mu(-\varepsilon') & f_\mu(\varepsilon',\varepsilon)+g_{\mu\mu}(\varepsilon',\varepsilon) \end{pmatrix}^{-1} \begin{pmatrix} \sqrt{2} \\ a_\mu(\varepsilon) \end{pmatrix}$$
$$+ \tfrac{1}{2}|A_\mu|^2(N_\mu+1)a^*_\mu(\varepsilon')[f_\mu(\varepsilon',\varepsilon)-g_{\mu\mu}(\varepsilon',\varepsilon)]^{-1}a_\mu(\varepsilon)\,. \tag{26}$$

The first and second terms of Eq. (26) arise from singlet and triplet two-hole final states of the $(N-1)$-electron system, respectively.

With $g^<(z)$ being the sum of $g^<_{\nu=\mu}(z)$ and $g^<_{\nu\neq\mu}(z)$, our results for the electron removal $d$-spectral weight are given by Eqs. (16)–(20), (24)–(26). Following Gunnarsson and Schönhammer,[40] we have discretized the interval $(0,B)$ in order to invert the matrices in Eqs. (25) and (26). We tested numerical functions of essentially zero width for $|V_\nu(\varepsilon)|^2$ to insure that the computer program would reproduce the analytic results for the cluster model discussed in Appendix B. Our results are presented in Figs. 5 and 6. They were obtained using 81 (Fig. 5) and 41 (Fig. 6) points in the interval $(0,B)$, and taking the imaginary part of $z$ to provide full width at half maximum Lorentzian broadening of 0.45 eV, the stated instrumental resolution of Shen *et al.*[50]

The solid and dotted curves in Fig. 5 were obtained us-

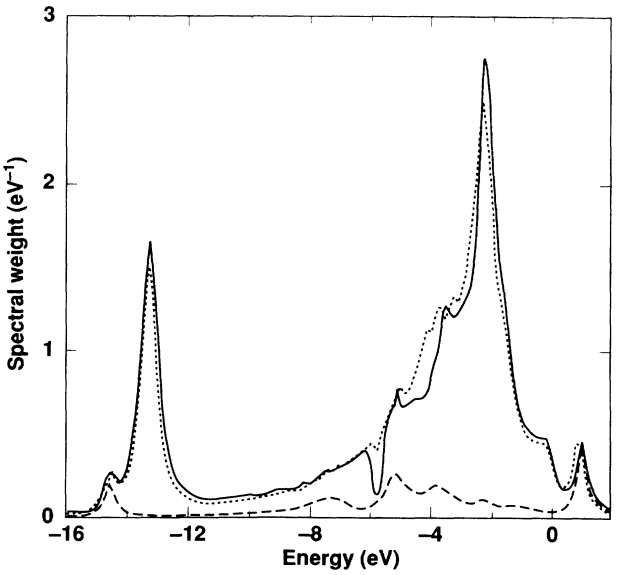


FIG. 5. Calculated impurity Anderson-model $d$ spectral weight for $La_2CuO_4$. Solid and dotted curves correspond to cases 1 and 2 of Table VI, respectively. The dashed curve gives just the $\nu=\mu=x^2-y^2$ contribution to the former.

ing the parameters appropriate to cases 1 and 2 of Table VI, respectively. The overall close agreement between the two curves shows limited sensitivity of the calculated $d$-spectral weight to the uncertainty in our Cu($3d$) Wannier function represented by the radius of the Cu sphere. In particular, the agreement in position of the predominantly $d^8$ peak near −13.5 eV is ≈0.05 eV, while the separate

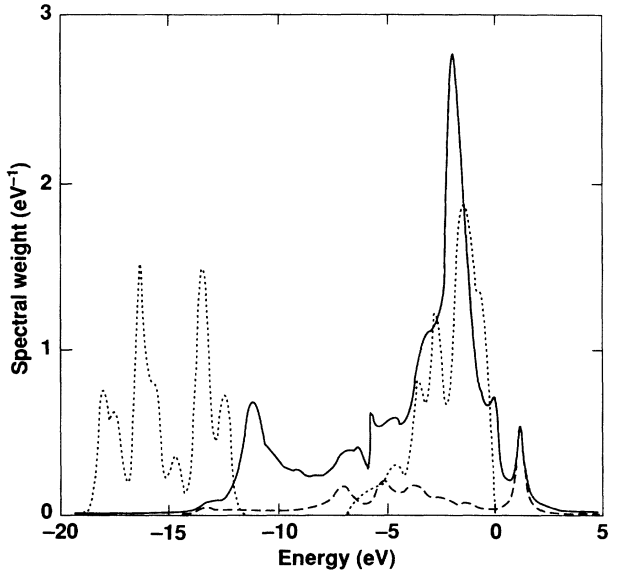


FIG. 6. Calculated impurity Anderson-model $d$ spectral weight (solid curve) based on case-3 parameters of Table VI, and broadened O($2s$), La($5p$), and O($2p$) local-density density of states (dotted curve) reduced by a factor of 5. The dashed curve gives the $\nu=\mu=x^2-y^2$ contribution to the former.

changes in $\underline{\varepsilon}_d$, $U_d$, and $|V_\mu(\varepsilon)|^2$ between cases 1 and 2 would shift this peak by −0.8, 0.5, and 0.2 eV, respectively.

Two points of qualitative agreement between our theoretical results in Fig. 5 and the photoemission data are to be noted. First, most of the $d$-spectral weight overlaps the O($2p$) states in the range from −6.7 to 0 eV, creating the large peak which dominates both theory and data. Second, a modest bump of $d$ character is seen in resonant PES measurements at about 11.5 eV below the top of the O($2p$) bands (which we take 1 eV below the Fermi level of Shen *et al.*[50]). We identify this structure with the predominantly $d^8$ peak near −13.5 eV in Fig. 5. Located near the edge of the two-hole continuum, the position and size of this peak are sensitive to the parameters. A reduction of $2\underline{\varepsilon}_d+U_d$ to 6.3 eV diminishes the size of the peak and moves it to higher energies as seen from the solid curve in Fig. 6, obtained with the case-3 parameters of Table VI. A similar result obtains with the case-4 parameters. The dotted lines in Fig. 6 show the one-electron density of states for comparison, O($2p$) at higher energies, and combined La($5p$) and O($2s$) at lower energies. These have been Gaussian broadened [full width at half maximum (FWHM) of 0.45 eV], and divided by 5, the rough matrix element reduction suggested for the O($2p$) states by Shen *et al.*[50] The onset of our spin-orbit split La($5p$) contribution for energies below −12 eV occurs at ≈2 eV higher energies than found in the PES data, a familiar problem with corelike one-electron eigenvalues as has been noted, e.g., for the $3d$ levels in GaAs.[66]

A realistic comparison with experiment of the calculated $d^8$ structure is premature given our scalar approximation to the true matrix nature of $U_d$. Antonides and Sawatzky[67] have noted that multiplet splittings in the solid can be (80–90)% of their atomic values. Since the large $^1$S splitting can affect only the $\nu=\mu=x^2-y^2$ contributions to the total spectral weight, given by the dashed curves in Figs. 5 and 6, the bulk of the $d^8$ structures in these figures would appear to be subject to multiplet splittings of about ±1.5 eV.[60]

Our primary interest in this paper is not the $d^8$ region, but rather the small peak in Figs. 5 and 6 lying ≈1 eV *above* the top of the O($2p$) band. This is a true pole in these impurity-model calculations, at an energy we shall call $E_{\rm PES}$ (weight $w_{\rm PES}$), which arises from the singlet, $x^2-y^2$ two-hole ground state of the $(N-1)$-electron system. It occurs both because of the large magnitude of the $x^2-y^2$ hybridization as well the pronounced strength of this coupling near the top of the O($2p$) band. While there is some uncertainty in the position of this peak, we emphasize that its existence and essential features are unaffected by the wide range of parameters explored in Table VI. We also note that lattice broadening of this peak would provide the kind of low density of states which is observed in photoemission spectroscopy.[49–43] There is a similar pole, by the way, for a $3z^2-r^2$, $x^2-y^2$ two-hole pair ≈0.1 eV above the top of the O($2p$) band.

We have solved for the two-$(x^2-y^2)$-hole singlet ground state $\Phi_g^{(N-1)}$ of the $(N-1)$-electron system in the same manner as in Eqs. (8)–(12) for the $N$-electron case, in order to determine the disposition of the two holes on

Cu and O sites ($w_{dd}$, $w_{pp}$, and $w_{pd}$) and the number of $d$ holes $\langle N-1|\underline{n}_d|N-1\rangle = 2w_{dd}+w_{pd}$ as given in Table VI. These calculations also give the more precise values for $E_{\rm PES}=E_{g\mu}^{(N)}-E_g^{(N-1)}$, and $w_{\rm PES}=|\langle\Phi_g^{(N-1)}|\psi_{\mu\downarrow}^{\dagger}|\Phi_{\mu\uparrow}^{(N)}\rangle|^2$, where $\mu=x^2-y^2$, which are reported in the table. As can be deduced from the difference $\langle N-1|\underline{n}_d|N-1\rangle-\langle N|\underline{n}_d|N\rangle$, the added hole in $\Phi_g^{(N-1)}$ is more than 80% O($2p$) in character, in agreement with recent data.[68,69] The state is highly correlated, with $w_{dd}=10\%$ or less probability of both holes being on the Cu impurity site. These impurity-model calculations suggest, therefore, that the first ionization level of $La_2CuO_4$ is a strongly correlated, $x^2-y^2$ symmetry two-hole singlet lying above the continuum of the electron removal spectrum. We do not believe this qualitative conclusion is comprised either by our neglect of multiplet structure,[70] or, at least within the context of the cluster calculations in Appendix B, by the possibility of a $U_p$ even as large as 7 eV.

## IV. SUMMARY AND DISCUSSION

We have presented *ab initio* calculations of the parameters defining a general effective Hamiltonian for $La_2CuO_4$ that we believe to be an appropriate starting point for many-body calculations in this material and by extension to other copper oxide superconductors. The principal results given in Table II are the parameters which enter the many-body interacting-electron Hamiltonian equation (4). This Hamiltonian may be reasonably approximated by an Anderson lattice model of the electronic structure of the new superconductors, i.e., Cu($3d$) states with large Coulomb interactions which are hybridized with broad oxygen $p$ bands. The Coulomb interactions $U_p$ and $U_{pd}$ are sufficiently small that we believe it is reasonable to neglect them, which is a crucial aspect of an Anderson-type model. The magnitude of $U_{pd}$ which we find is smaller than that in Refs. 21 and 22 needed to cause superconductivity. Our conclusions support the applicability of two (or more) band models in which holes interact with spins (Refs. 12–16) and the Anderson lattice model of Refs. 17 and 18. As discussed below, we believe several states are possibilities for the holes—including the mainly O($2p$) states of $d_{x^2-y^2}$ symmetry (as in Refs. 12 and 13) the $p_\pi$ states of $g_{xy(x^2-y^2)}$ symmetry (as in Refs. 15 and 16), and states with $d_{3z^2-r^2}$ symmetry—and that further many-body calculations are needed to select among these possibilities.

Among the parameters in Table II we believe the most uncertain are $U_p$ (as discussed in Sec. II) and the energy of the Cu($3d$) state relative to the oxygen band. The reasons for potential uncertainties in the relative $d$-$p$ energies are twofold: First, because of the different character of these states, one may expect the density functional to make errors in the difference between their energies. In the case of $CeO_2$ and $PrO_2$, we argued[43] that the calculated $4f$-$2p$ separations were too small by $\approx 1$ eV. Second, there are possibilities for errors in the very different ways we have treated $U_d$ and $U_p$, which could renormalize the $\varepsilon_d-\varepsilon_p$ energies. We note that whereas we have placed the $d^9\rightarrow d^{10}$ energy near the edge of the O bands, Newns and co-workers[17,18] have argued that the $d$ state should be $\approx 2$ eV higher (lower) than the edge of the O bands for electrons (holes).

We have also solved our proposed Hamiltonian in the impurity approximation. A convenient summary of the excitation spectra predicted by our impurity-model calculations is given by the densities of states sketched in Fig. 7, which provide visual identification of the quantities presented in Table VI. Stoichiometric $La_2CuO_4$ has one hole per unit cell relative to filled Cu($3d$) levels and O($2p$) bands. It is approximated within the impurity model by one hole associated with a single Cu atom embedded in the O lattice. The ground-state energy $E_g^{(N)}=\Delta E_{x^2-y^2}$ of this $N$-electron system occurs when the hole occupies an antibonding Cu($3d$)-O($2p$) hybrid of $x^2-y^2$ symmetry about the Cu site, the level to the far right in Fig. 7(a). This state is magnetic in agreement with experimental observations on $La_2CuO_4$ and related materials.[7,8] The hole may be excited to crystal-field levels of other symmetries at higher energies $-\Delta E_\mu$ to the left in Fig. 7(a), and finally into the uncoupled O($2p$) continuum. Bearing in mind that these levels may broaden considerably due to lattice effects, the excitations evident in Fig. 7(a) are qualitatively the same as those proposed by Geserich *et al.*[63] to explain their reflectivity data for $YBa_2Cu_3O_{7-\delta}$. These authors invoke electron quadrupole selection rules to allow the otherwise forbidden $d$-$d$ crystal field excitations. For $La_2CuO_4$, we would expect from Table VI to have crystal-field excitations at $\approx 1.4$ eV ($3z^2-r^2$) and $\approx 2$ eV ($yz$, $zx$, and $xy$ combined), and a charge-transfer gap[71] $|\Delta E_{x^2-y^2}|=2$–3 eV.

The true many-body nature of the present impurity-model calculations is evident in the difference between Figs. 7(a) and 7(b). The latter sketches the densities of

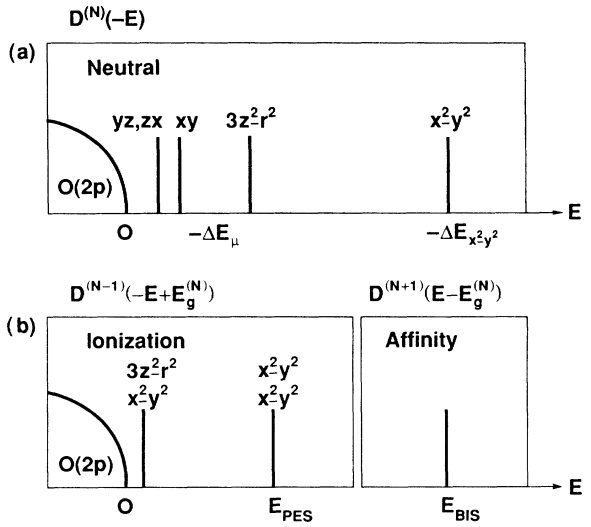


FIG. 7. Sketches of the impurity-model state densities for $La_2CuO_4$ near the Fermi level. (a) Crystal-field excitations for the one hole (per unit cell in the lattice) in the stoichiometric or neutral material ($N$-electron system, ground-state energy $E_g^{(N)}=\Delta E_{x^2-y^2}$). (b) Electron ionization [$(N-1)$-electron] and affinity [$(N+1)$-electron] spectra showing an insulating gap and hole-particle excitations for the neutral material. Note the energy $E_{\rm PES}$ to add a second $d_{x^2-y^2}$ hole in (b) is significantly shifted from the energy $-\Delta E_{x^2-y^2}$ to add the first such hole in (a).

electron ionization and affinity levels near the Fermi level, and would be identical to Fig. 7(a) were $U_d=0$. In particular, were $U_d=0$, the minimum energy to add a hole $E_{\rm PES}$ would equal the minimum energy to add an electron $E_{\rm BIS}$ which is just the energy $-\Delta E_{x^2-y^2}$ in Fig. 7(a). As it is, we find a correlation gap $E_{\rm gap}=E_{\rm BIS}-E_{\rm PES}=1.3\pm0.3$ eV making stoichiometric $La_2CuO_4$ an insulator assuming lattice broadening of the two levels is not sufficient to fill in the gap. This gap implies particle-hole excitations of the $N$-electron system which must be considered in addition to the crystal-field-like excitations of the preexisting hole in each unit cell evident in Fig. 7(a). Such particle-hole excitations might annihilate a hole in one unit cell, leaving two holes in another, and have comparable energy as can be seen from Fig. 7(b). Electron-hole interactions would further reduce this energy.

We have suggested that lattice broadening of the levels labeled $E_{\rm PES}$ and $E_{\rm BIS}$ in Fig. 7(b) might account for the low spectral weight observed in PES and BIS experiments near the Fermi level, between the large O($2p$)-Cu($3d$) structure below, and the La($4f$,$5d$) states above. Figure 1(b) suggests the latter begin about 2 eV above the top of the O bands. However, local-density theory can be expected to underestimate the O($2p$)-La($4f$,$5d$) separation, and indeed we find the center of our La($4f$) bands far lower relative to the dominant O($2p$) and Cu($3d$) contribution than observed in the PES and BIS data. Therefore, we expect the La($4f$,$5d$) levels to begin 4 eV or more above the top of the O bands, and have therefore omitted these states from Fig. 7. At more negative energies, our calculated $d$ spectral weight is in qualitative agreement with the PES data in regard to the dominant $\approx$7-eV-wide peak of Cu($3d$) and O($2p$) character beginning just below the Fermi level, and a more distant, weaker peak of predominantly $d^8$ character.

The ionization states in Fig. 7(b) may also be viewed in terms of the doped-in holes in $La_{2-x}Sr_xCuO_4$, and the results are qualitatively the same as found by Newns and co-workers[18] in their $1/N$ expansion treatment of the Anderson lattice Hamiltonian for this material. They find $\approx$1-eV-wide $d_{x^2-y^2}$ and $d_{3z^2-r^2}$ bands lying above the itinerant O($2p$) bands, which are shifted towards the O bands by the increased hole concentration. This is precisely the change seen from Fig. 7(a) ($x=0$) to the ionization part of Fig. 7(b) ($x=1$), where the first $x^2-y^2$ hole is added at $-\Delta E_{x^2-y^2}$, and the second at $E_{\rm PES}$, more than 1 eV closer to the O band. At $x=0.12$, Newns and co-workers find the Fermi level moves into the itinerant band.[18] Even prior to this, however, they find as do we that added holes in the $d_{x^2-y^2}$ band or level are (75–80)% of O($2p$) character, in agreement with analyses of PES[68] and low-energy electron-diffraction spectroscopy[69] data.

It should be noted that the two $x^2-y^2$ hole state at $E_{\rm PES}$ in Fig. 7(b) is a singlet, and that the addition energy for a second hole in a triplet configuration would lie at much higher hole energies overlapping the O bands. Thus $E_{\rm PES}$ ($\sim$1 eV for $U_p=0$, $\sim$0.4 eV for $U_p=7.3$ eV, see Appendix B) provides an estimate of the antiferromagnetic exchange interaction between the two holes. Although our impurity-model calculations have not dealt with magnetic order, or interactions between holes in different unit cells, the possibility that doped in holes may form singlet composites in cooperation with preexisting holes is suggestive of the spinless, charged holons in the resonating-valence-bond picture.[9–11] However, we believe these states are more accurately described as hole-spin pairs in a two-band picture[12–16] rather than the absence of a spin in a one-band picture.[9–11]

We conclude this section with speculations about the nature of the carrier states in $La_{2-x}Sr_xCuO_4$ in light of the present impurity-model results, and the likely corrections to these calculations dictated by the full effective Hamiltonian of Sec. II. Lattice effects appear to lead to widths $\approx$1 eV of the $d_{x^2-y^2}$ and $d_{3z^2-r^2}$ levels in Fig. 7, judging from the work of Newns and co-workers,[18] and, based on calculations incorporating nearest-neighbor Cu sites, they may be expected to increase the insulating gap by raising both the energies to add holes and electrons.[72] The cluster calculations of Appendix B also suggest some increase in the gap due to $U_p$. As the $x^2-y^2$ states are driven further from the Fermi level by these effects, the possibility is raised of either relatively pure O($2p$) or Cu-O hybrid $3z^2-r^2$ states becoming the states where the added holes will reside. Even if this possibility is not realized, however, and the added holes go into $x^2-y^2$ states as suggested by Fig. 7(b), our results do not support a one-band Hubbard model due to the significantly different character of the added holes ($\approx$80% O) and electrons ($\approx$60% Cu).

*Note in proof*: We have recently learned that K. T. Park, K. Terakura, T. Oguchi, A. Yanase, and M. Ikeda find similar tight-binding parameters to our results in Table II, and that H. Eskes and G. A. Sawatzky have also performed impurity Anderson model calculations which predict a two-hole singlet for the first ionization level. If the singlet binding energy is sufficiently strong, Zhang and Rice [F.C. Zhang and T. M. Rice, Phys. Rev. B **37**, 3759 (1988)] argue that the effective Hamiltonian can be reduced to a one-band Hubbard model.

## ACKNOWLEDGMENTS

The authors have benefited from conversations with J. W. Allen, J. F. Annett, D. R. Hamann, B. N. Harmon, C. Herring, M. S. Hybertsen, D. R. Jennison, D. M. Newns, and M. Schlüter. One of us (R.M.M.) acknowledges many helpful discussions with his colleagues at the University of Illinois. This work has been supported at Lawrence Livermore National Laboratory by Contract No. W-7405-ENG-48 to the U.S. Department of Energy and at the University of Illinois by National Science Foundation Grant No. DMR-86. Part of this work was done while two of the authors (R.M.M. and S.S.) were at Xerox Palo Alto Research Center, where it was supported in part by the U.S. Office of Naval Research under Contract No. N00014-82-C-0244.

## APPENDIX A: CRYSTAL-FIELD AND SPIN-ORBIT EFFECTS

In the present LMTO calculations, in which the states are solutions of Schrödinger equations in spherically sym-

metrized potentials in each sphere, the only splitting and dispersion of the $d$ states results from coupling to neighboring spheres, i.e., hybridization. However, as noted by Chan and Lam,[73] hybridization of the localized orbitals with the valence bands is only one source of crystal field, and one must also consider that due to lattice-point charges. This separation is clearly basis dependent, as is particularly evident in the context of choosing the sphere sizes in the LMTO approach. The relatively large Cu and La spheres in Table I, for example, result in small net sphere charges, the largest being $0.44e$ for the La sphere, contributing in part to a small point-charge contribution to the crystal field.

The electrostatic multipole field at the Cu site is simply calculated from the net charges of the surrounding LMTO spheres, which may be collapsed to point charges given their imposed spherical symmetry. Using selected $\mathbf{k}=\mathbf{0}$ LMTO structure constants to obtain the Madelung sums,[74] and averages $\langle r^n \rangle$ over the radial Cu($3d$) orbitals, we find coefficients $-0.064$, 0.055, and 0.057 eV, respectively, of the spherical harmonics $Y_2^0(\hat{r})$, $Y_4^0(\hat{r})$, and $Y_4^{\pm 4}(\hat{r})$, in an expansion of the multipole potential. This potential implies shifts of 0.033 $(x^2-y^2)$, 0.002 $(3z^2-r^2)$, $-0.006$ $(xy)$, and $-0.015$ eV $(yz,zx)$ which are negligible compared to hybridization effects $\approx 1$ eV.

For the band-center logarithmic derivative, we calculate the spin-orbit splitting of the Cu($3d$) orbital to be $\varepsilon_d(j=5/2)-\varepsilon_d(j=3/2)\approx 0.3$ eV in $La_2CuO_4$. This is much smaller than the $\approx 1$ eV hybridization splitting of the levels mentioned above. Moreover, while the spin-orbit interaction may split $yz,zx$ levels in first order, it can only shift $x^2-y^2$ and $3z^2-r^2$ levels in second or higher order. We estimate these shifts to be $\approx 0.03$ eV, and therefore do not include the spin-orbit interaction in the present work.

## APPENDIX B: CLUSTER CALCULATION INCLUDING $U_p$ AND $U_{pd}$

In this appendix we use a cluster model to accurately reproduce the first ionization and affinity levels predicted for $La_2CuO_4$ by the impurity Anderson model calculations of Sec. III, a treatment made possible by the discrete nature of these levels lying outside of the O($2p$) continuum. The cluster model then permits simple inclusion of the Coulomb interactions $U_p$ between two holes on the same O site, and $U_{pd}$ between holes on neighboring Cu and O sites. We find that the effect of these interactions is to depress the first ionization level, increasing the insulating gap by up to 30%, while leading to a more strongly correlated two-hole state. The essential qualitative conclusion of Sec. III is unchanged, namely, that the first ionization level of $La_2CuO_4$ is a strongly correlated, $x^2-y^2$ symmetry two-hole singlet lying above the continuum of the electron removal spectrum.

We take the Hamiltonian for the cluster model in the form

$$H=\underline{\varepsilon}_p\sum_\tau p_\tau^\dagger p_\tau+\underline{\varepsilon}_d\sum_\tau d_\tau^\dagger d_\tau+U_p\sum_i\sum_{\substack{\sigma,\tau\\ \sigma<\tau}} n_{i\sigma}^{(p)}n_{i\tau}^{(p)}+U_d\sum_{\substack{\sigma,\tau\\ \sigma<\tau}} n_\sigma^{(d)}n_\tau^{(d)}+U_{pd}\sum_{\sigma,\tau} n_\sigma^{(p)}n_\tau^{(d)}+V\sum_\tau (d_\tau^\dagger p_\tau+\text{H.c.})\,, \tag{B1}$$

where $p_\tau^\dagger$ ($d_\tau^\dagger$) creates an O (Cu) hole of spin $\tau$ and energy $\underline{\varepsilon}_p$ ($\underline{\varepsilon}_d$) and $V$ is the hybridization between these states. The Coulomb interactions are $U_p$, $U_d$, and $U_{pd}$. We are interested only in the important $x^2-y^2$ symmetry case, and therefore take $V=3.2$ eV, which is the square root of the area under the $|V_{x^2-y^2}(\varepsilon)|^2$ curve in Fig. 4. Furthermore, to make contact with the impurity model we would like $p_\tau^\dagger$ to create a molecular orbital having amplitude on all four O sites surrounding the Cu in the $CuO_2$ layer, i.e.,

$$p_\tau^\dagger \equiv \tfrac{1}{2}\sum_i c_i p_{i\tau}^\dagger\,. \tag{B2}$$

Here, $i$ runs over the four O sites, and $c_i$ are the appropriate phases required to give the molecular-orbital $x^2-y^2$ symmetry about the Cu site. Since $U_p$ should only pertain to two holes on the same O site, Eq. (B1) involves $n_{i\tau}^{(p)}\equiv p_{i\tau}^\dagger p_{i\tau}$; whereas elsewhere in the equation, the composite operators $p_\tau$ and $p_\tau^\dagger$ are used.

The ground state of the $N$-electron system, i.e., one hole in the $CuO_4$ cluster, is easily found in a manner similar to Sec. III. Taking first $U_p=U_{pd}=0$ (also $U_d=8.5$ eV, and $\underline{\varepsilon}_d=0.4$ eV) we choose the O hole energy $\underline{\varepsilon}_p=1.19$ eV so that the solution reproduces the same 0.56 probability for the hole being on the Cu site as was found for the impurity Anderson model. With this single empirical choice of $\underline{\varepsilon}_p$, the cluster-model results for the ground states of the $N$- and $(N-1)$-electron systems shown in Table VII

TABLE VII. Cluster-model calculations for $La_2CuO_4$. *$N$-electron (one-hole) ground state:* Total energy $\Delta E$ and number of $d$ holes $\langle N|\underline{n}_d|N\rangle$ are given. *$(N-1)$-electron (two-hole) ground state:* The probabilities of both holes being on the Cu site ($w_{dd}$), the same O site ($w_{pp}$), different O sites ($w_{p'p}$), or one each on the Cu and an O site ($w_{pd}$) are given along with the number of $d$ holes $\langle N-1|\underline{n}_d|N-1\rangle$. The first ionization energy is $E_{\rm PES}$ ($d$ spectral weight $w_{\rm PES}$). *$(N+1)$-electron ground state:* The first affinity level is $E_{\rm BIS}$ ($d$ spectral weight $w_{\rm BIS}$). The insulating gap is $E_{\rm gap}$. All calculations assumed $\underline{\varepsilon}_d=0.4$ eV, $\varepsilon_p=1.19$ eV, $V=3.2$ eV, and $U_d=8.5$ eV. All energies are in eV.

| Quantity | Case 1 | Case 2 |
|---|---|---|
| $U_p$ | 0 | 7.3 |
| $U_{pd}$ | 0 | 0.6 |
| | $N$-electron system | |
| $\Delta E=-E_{\rm BIS}$ | $-2.43$ | $-2.43$ |
| $\langle N\|\underline{n}_d\|N\rangle=w_{\rm BIS}$ | 0.56 | 0.56 |
| | $(N-1)$-electron system | |
| $w_{dd}$ | 0.07 | 0.08 |
| $w_{pp}$ | 0.09 | 0.02 |
| $w_{p'p}$ | 0.26 | 0.32 |
| $w_{pd}$ | 0.58 | 0.58 |
| $\langle N-1\|n_d\|N-1\rangle$ | 0.72 | 0.74 |
| $E_{\rm PES}$ | 1.07 | 0.42 |
| $w_{\rm PES}$ | 0.31 | 0.32 |
| $E_{\rm gap}$ | 1.36 | 2.01 |

(case 1) are in rather striking agreement with the corresponding impurity Anderson model quantities in Table VI (case 1). This is especially true for the decomposition of the $(N-1)$-electron ground state to be discussed momentarily, but even the positions $E_{\rm BIS}$ and $E_{\rm PES}$ of the electron affinity and ionization levels which bound the insulating gap agree to $\approx 0.1$ eV.

To find the ground state of Eq. (B1) for the $(N-1)$-electron or two-hole case, we consider only singlets, taking the basis

$$|dd\rangle \equiv d_{\downarrow}^{\dagger} d_{\uparrow}^{\dagger} |0\rangle , \tag{B3a}$$

$$|pp\rangle \equiv \tfrac{1}{2} \sum_i c_i^2 p_{i\downarrow}^{\dagger} p_{i\uparrow}^{\dagger} |0\rangle , \tag{B3b}$$

$$|p'p\rangle \equiv \frac{1}{\sqrt{12}} \sum_{\substack{i,j \\ i \neq j}} c_i c_j p_{i\downarrow}^{\dagger} p_{j\uparrow}^{\dagger} |0\rangle , \tag{B3c}$$

$$|pd\rangle \equiv \frac{1}{\sqrt{2}} (d_{\downarrow}^{\dagger} p_{\uparrow}^{\dagger} + p_{\downarrow}^{\dagger} d_{\uparrow}^{\dagger}) |0\rangle . \tag{B3d}$$

The weights $w_{dd}$, $w_{pp}$, $w_{p'p}$, and $w_{pd}$ in Table VII are the squares of the amplitudes of these states corresponding to the ground-state eigenvalue $E_g^{(N-1)}$ of the $4\times 4$ matrix resulting from this basis. The location of the first ionization level $E_{\rm PES} = E_g^{(N)} - E_g^{(N-1)}$ is the difference between $N$- and $(N-1)$-electron ground-state energies, while the strength of this state in the $d$-spectral weight is $w_{\rm PES} = |\langle \Phi_g^{(N-1)} | d_{\downarrow}^{\dagger} | \Phi_{g\uparrow}^{(N)} \rangle|^2$, taking the hole in the $N$-electron ground state to be spin up.

The agreement between the cluster (case 1, Table VII) and impurity Anderson (case 1, Table VI) models for the weights $w$ related to the $(N-1)$-electron system ground state is 0.02 or better. The 0.35 probability for two O holes in Table VII is decomposed into $w_{pp}$ and $w_{p'p}$ corresponding to whether the holes are on the same or different O sites, respectively. For $U_p = 0$, there is no correlation between the two holes when they are both on O sites, and so $w_{p'p} = 3w_{pp}$ exactly.

Having established that the cluster model can reproduce the first ionization and affinity levels of the impurity Anderson model when $U_p = U_{pd} = 0$, we can now repeat the solution with our Sec. II estimates for these quantities as shown in case 2 of Table VII. As can be seen by comparison of the two columns in Table VII, the predominant effect is an onset of correlation between the two holes when they are both on O sites, so there remains little probability $w_{pp}$ of both being on the same O site, although the sum $w_{pp} + w_{p'p}$ is nearly unchanged. Finite $U_p$ does raise the total energy $E_g^{(N-1)}$, shifting $E_{\rm PES}$ by $-0.65$ eV, and increasing the insulating gap to $\approx 2$ eV for the extreme case of $U_p = 7.3$ eV. If applied directly to the impurity model, this shift in $E_{\rm PES}$ still leaves the two-$(x^2-y^2)$-hole singlet closer to the Fermi energy than the O$(2p)$ continuum located at $E < 0$. Furthermore, neglected effects of $U_p$ on these O$(2p)$ states may shift this continuum to even more negative energies.

These cluster calculations are certainly over simplified. However, we suggest that the qualitative conclusion is correct, namely, that the effect of $U_p$ is to enhance correlation effects in the first ionization state of $La_2CuO_4$ while increasing the insulating gap, but that in itself $U_p$ is not sufficient to move pure O states closer to the Fermi level than the Cu-O hybrid, two-hole, $x^2-y^2$ symmetry singlet.


[1] N. F. Mott, *Metal-Insulator Transitions* (Taylor & Francis, London, 1964).

[2] Examples of recent conference proceedings on correlated electron systems are *Proceedings of the International Conference on Valence Fluctuations,* edited by E. Muller-Hartmann, B. Roden, and D. Wohlleben (North-Holland, Amsterdam, 1985), and Ref. 3.

[3] *Proceedings of the XVIII Yamada Conference on Superconductivity in Highly Correlated Fermion Systems* [Physica B+C **148**, Nos. 1-3 (1987)].

[4] J. G. Bednorz and K. A. Müller, Z. Phys. B **64**, 189 (1986).

[5] M. K. Wu, J. R. Ashburn, C. J. Torng, P. H. Hor, R. L. Meng, L. Gao, Z. J. Huang, Y. Q. Wand, and C. W. Chu, Phys. Rev. Lett. **58**, 908 (1987).

[6] See papers in *Proceedings of the International Conference on High Temperature Superconductors and Materials and Mechanisms of Superconductivity, Interlaken, Switzerland, 1988* [Physica C **153–155** (1988)].

[7] S. Mitsuda, G. Shirane, S. K. Sinha, D. C. Johnston, M. S. Alvarez, D. Vaknin, and D. E. Moncton, Phys. Rev. B **36**, 822 (1987); D. Vaknin, S. K. Sinha, D. E. Moncton, D. C. Johnston, J. M. Newsam, C. R. Safinya, and H. E. King, Jr., Phys. Rev. Lett. **58**, 2802 (1987).

[8] R. J. Birgeneau *et al.* (unpublished).

[9] P. W. Anderson, Science **235**, 1196 (1987).

[10] G. Baskaran, Z. Zou, and P. W. Anderson, Solid State Commun. **63**, 973 (1987); P. W. Anderson, G. Baskaran, Z. Zou, and T. Hsu, Phys. Rev. Lett. **58**, 2790 (1987); P. W. Anderson and Z. Zou, *ibid.* **60**, 132 (1988).

[11] S. A. Kivelson, D. S. Rokhsar, and J. P. Sethna, Phys. Rev. B **35**, 8865 (1987); S. A. Kivelson and D. S. Rokhsar, in Ref. 6; V. Kalmeyer and R. B. Laughlin, Phys. Rev. Lett. **59**, 2095 (1987); R. B. Laughlin, Science (to be published).

[12] V. J. Emery, Phys. Rev. Lett. **58**, 2794 (1987).

[13] J. E. Hirsch, Phys. Rev. Lett. **59**, 228 (1987).

[14] J. R. Schrieffer, X.-G. Wen, and S.-C. Zhang, Phys. Rev. Lett. **60**, 944 (1988).

[15] Y. Guo, J.-M. Langlois, and W. A. Goddard III, Science **239**, 896 (1988); G. Chen and W. A. Goddard III, *ibid.* **239**, 899 (1988).

[16] R. J. Birgeneau, M. A. Kastner, and A. Aharony, Z. Phys. B **71**, 57 (1988).

[17] D. M. Newns, Phys. Rev. B **36**, 5595 (1987); D. M. Newns and M. Rasolt, *ibid.* (to be published).

[18] D. M. Newns, P. Pattnaik, M. Rasolt, and D. A. Papaconstantopoulos (unpublished); this work uses a parametrized band structure due to D. A. Papaconstantopoulos, M. J. DeWeert, and W. E. Pickett, in *High Temperature Superconductors,* edited by M. B. Brodsky *et al.*, MRS Symposia Proceedings No. 99 (Materials Research Society, Pittsburgh, PA, 1988).

[19] P. A. Lee, G. Kotliar, and N. Reed, Physica B **148**, 274 (1987).

[20] C. M. Varma, S. Schmitt-Rink, and E. Abrahams, Solid State Commun. **62**, 681 (1987).

[21] J. E. Hirsch, E. Loh, D. J. Scalapino, and S. Tang, in Ref. 6.

[22] J. E. Hirsch, S. Tang, E. Loh, Jr., and D. Scallapino, Phys.

Rev. Lett. **60**, 1668 (1988).
[23]H. B. Schüttler, Phys. Rev. B **38**, 2854 (1988).
[24]W. Harrison, in *Novel Superconductivity,* edited S. A. Wolf and V. Z. Kresin (Plenum, New York, 1987), p. 507; and Phys. Rev. B **38**, 270 (1988).
[25]J. Yu, S. Massidda, A. J. Freeman, and D. D. Koelling, Phys. Lett. A **122**, 203 (1987).
[26]W. Weber, Z. Phys. B **70**, 323 (1988).
[27]E. B. Stechel and D. R. Jennison, Phys. Rev. B (to be published).
[28]W. Kohn and L. J. Shan, Phys. Rev. **140**, A1133 (1965).
[29]See papers in *Theory of the Inhomogeneous Electron Gas,* edited by S. Lundquist and N. H. March (Plenum, New York, 1983).
[30]A review of density functional calculations is given by R. M. Martin, Festkörperprobleme **25**, 3 (1985).
[31]L. F. Mattheiss, Phys. Rev. Lett. **58**, 1028 (1987).
[32]J. Yu, A. J. Freeman, and J.-H. Xu, Phys. Rev. Lett. **58**, 1035 (1987).
[33]K. Takegahara, H. Harima, and A. Yanase, Jpn. J. Appl. Phys. **26**, L352 (1987).
[34]T. Oguchi, Jpn. J. Appl. Phys. **26**, L417 (1987).
[35]W. E. Pickett, H. Krakauer, D. A. Papaconstantopoulos, and L. L. Boyer, Phys. Rev. B **35**, 7252 (1987).
[36]R. V. Kasowski, W. Y. Hsu, and F. Herman, Solid State Commun. **63**, 1077 (1987); and Phys. Rev. B **36**, 7248 (1987).
[37]D. M. Ceperley and B. J. Alder, Phys. Rev. Lett. **45**, 566 (1980); D. Ceperley and B. Alder, Science **231**, 555 (1986).
[38]For Monte Carlo calculations applied to problems related to the Cu-O systems, see, for example, J. E. Hirsch, Phys. Rev. Lett. **59**, 228 (1987), and Refs. 21 and 22.
[39]Reference 15 provides an example of configuration interaction techniques applied to the Cu-O systems.
[40]O. Gunnarsson and K. Schönhammer, Phys. Rev. B **28**, 4315 (1983).
[41]See review by N. E. Bickers, Rev. Mod. Phys. **59**, 845 (1987).
[42]P. A. Lee, T. M. Rice, J. W. Serene, L. J. Sham, and J. W. Wilkins, Comments Condens. Mater. Phys. **12**, 99 (1986).
[43]A. K. McMahan and R. M. Martin, in *Narrow-Band Phenomena,* edited by J. C. Fuggle, G. A. Sawatzky, and J. W. Allen (Plenum, New York, 1988), p. 133.
[44]A. J. Freeman, B. I. Min, and M. R. Norman, in *Handbook on the Physics of Rare Earths,* edited by K. A. Gschneidner, L. Eyring, and S. Hafner (Elsevier, New York, 1987), Vol. 10, p. 165.
[45]O. Gunnarsson, O. K. Andersen, O. Jepsen, and J. Zaanen, in *Proceedings of the Tenth Tanigashi Symposium on Core Level Spectroscopies* (Springer, Berlin, in press).
[46]M. R. Norman and A. J. Freeman, Phys. Rev. B **33**, 8896 (1986).
[47]C. F. Chen, X. W. Wang, T. C. Leung, and B. N. Harmon (unpublished).
[48]M. Schlüter, M. S. Hybertsen, and N. E. Christensen, in Ref. 6.
[49]A. Fumjimori, E. Takayama-Muromachi, Y. Uchida, and B. Okai, Phys. Rev. B **35**, 8814 (1987).
[50]Z.-X. Shen, J. W. Allen, J. J. Yeh, J.-S. Kang, W. Ellis, W. Spicer, I. Lindau, M. B. Maple, Y. D. Dalichaouch, M. S. Torikachvili, J. Z. Sun, and T. H. Geballe, Phys. Rev. B **36**, 8414 (1987).
[51]N. Nücker, J. Fink, B. Reenkar, D. Ewert, C. Politis, P. J. W. Weijs, and J. C. Fuggle, Z. Phys. B **67**, 9 (1987).
[52]P. Steiner, J. Albers, V. Kinsinger, I. Sander, B. Siegwart, S. Hüfner, and C. Politis, Z. Phys. B **66**, 275 (1987).
[53]B. Reihl, T. Riesterer, J. G. Bednorz, and K. A. Müller, Phys. Rev. B **35**, 8804 (1987).
[54]O. K. Andersen, Phys. Rev. B **12**, 3060 (1975); O. K. Andersen and O. Jepsen, Physica B **91**, 317 (1977).
[55]H. L. Skriver, *The LMTO Method* (Springer, Berlin, 1984).
[56]O. K. Andersen and O. Jepsen, Phys. Rev. Lett. **53**, 2571 (1984); O. K. Andersen, O. Jepsen, and D. Glötzel, in *Highlights in Condensed Matter Theory,* edited by F. Bassani, F. Fumi, and M. P. Tosi (North Holland, New York, 1985).
[57]U. von Barth and L. Hedin, J. Phys. C **5**, 1629 (1972).
[58]W. A. Harrison, *Electronic Structure and the Properties of Solids* (Freeman, San Francisco, 1980), Sect. 2-D.
[59]J. C. Slater and G. F. Koster, Phys. Rev. **94**, 1498 (1954), see Table I; Ref. 58, Table 20-1. We use Harrison's notation for the Slater-Koster parameters, e.g., $V_{pd\sigma}$ for $(pd\sigma)$. Both references denote the actual hybridization matrix elements as, for example, $E_{x,x^2-y^2}$.
[60]C. E. Moore, *Atomic Energy Levels,* Circ. No. NBS 467 (U.S. GPO, Washington, DC, 1952), Vol. I, p. 45; Vol. II, p. 111. Our Table III is based on average configuration energies. The observed Cu $3d^8 4s^2$ multiplets are 5.84 ($^1S$), 1.64 ($^1G$), 0.77 ($^3P$), 0.38 ($^1D$), and $-1.40$ eV ($^3F$), relative to the average configuration energy.
[61]J. F. Herbst, R. E. Watson, and J. W. Wilkins, Phys. Rev. B **17**, 3089 (1978).
[62]P. H. Dederichs, S. Blügel, R. Zeller, and H. Akai, Phys. Rev. Lett. **53**, 2512 (1984).
[63]H. P. Geserich, G. Scheiber, J. Geerk, H. C. Li, G. Linker, W. Assmus, and W. Weber, Europhys. Lett. (to be published).
[64]U. Venkateswaran, K. Syassen, Hj. Mattausch, and E. Schönherr, Bull. Am. Phys. Soc. **33**, 473 (1988).
[65]R. Sooryakumar (private communication).
[66]G. B. Bachelet and N. E. Christensen, Phys. Rev. B **31**, 879 (1985).
[67]E. Antonides and G. A. Sawatzky, in *Transition Metals 1977,* edited by M. J. G. Lee, J. M. Perz, and E. Fawcett, Institute of Physics Conference Series No. 39 (Institute of Physics, Bristol, 1978), p. 134.
[68]A. Fujimori, E. Takayama-Muromachi, and Y. Uchida, Solid State Commun. **6**, 857 (1987).
[69]N. Nücker, J. Fink, J. C. Fuggle, P. J. Durham, and W. M. Temmerman, Phys. Rev. B **37**, 5158 (1988).
[70]A two-hole $x^2-y^2$ singlet state of a Cu ($3d^8$) ion would lie 2 eV above the configuration average, based on its $^1G$, $^1D$, $^1S$ decomposition and the multiplet positions in Ref. 60. If the two holes in $La_2CuO_4$ have only a 10% probability of both being on the same Cu site, one might anticipate only $\approx 0.2$ eV effects.
[71]J. Zaanen, G. A. Sawatzky, and J. W. Allen, Phys. Rev. Lett. **55**, 418 (1985).
[72]J. F. Annett, R. M. Martin, A. K. McMahan, and S. Satpathy (unpublished).
[73]S.-K. Chan and D. J. Lam, in *The Actinides,* edited by A. J. Freeman and J. B. Darby, Jr. (Academic, New York, 1974), Vol. I, see discussion on p. 11.
[74]The approach used here was pointed out to us by O. K. Andersen.